2009

VITAMIN B6 METABOLISM AND REGULATION OF PYRIDOXAL KINASE

Amit Gandhi
Virginia Commonwealth University

VITAMIN B_6 METABOLISM AND REGULATION OF PYRIDOXAL KINASE

A dissertation submitted in partial fulfillment of the requirements for the degree of Doctor of Philosophy at Virginia Commonwealth University.

By

AMIT K. GANDHI
M.S (Pharmaceutical Science), Rajiv Gandhi University, Indore, India, 2003
B.Pharm, Rajiv Gandhi University, Indore, India, 2001

Director: Martin K. Safo, Ph.D
Assistant Professor, Department of Medicinal Chemistry

Virginia Commonwealth University
Richmond, Virginia
December, 2009

Acknowledgement

I would like to take this opportunity to express my deep gratitude and profound respect to my advisor, Dr. Martin K. Safo, for his supervision, advice, and guidance in this research work. His support and insight have been invaluable in the progression of my research. I also appreciate his words of encouragement, which kept me always in an innovative mood and guided me at all the times to bring about the best in me. He is my mentor and teacher whom I shall remember forever.

I sincerely acknowledge Dr. Jason P. Rife, Dr. Glen E. Kellogg, Dr. Darrell L. Peterson and Dr. Walter M. Holmes for serving as my graduate committee members and for their advice, supervision, and support throughout my research.

I extend my sincere thanks to Dr. Faik N. Musayev for teaching me various protein purification and crystallographic techniques. My heartfelt thanks go to Dr. Mohini S. Ghatage, who helped me in protein expression, purification, and enzyme kinetic studies. . I would like to thank Dr. Richmond Danso-Danquah, who helped me in synthesis studies.

I gratefully acknowledge Dr. Verne Schirch for his constant guidance and motivation throughout my research. I would also like to convey my regards and thanks to Dr. Donald J. Abraham, for the financial support provided to me.

I can not express my emotions to my family, my wife, my parents, and my brother, who have provided countless moments of inspiration and motivation to achieve my goals. I also owe thanks to my all friends and all my well wishers, who have always inspired me for success.

I also thank Institute for Structural Biology and Drug Discovery (ISBDD) for providing me all the necessary facilities and resources. Finally, I am grateful to the Department of Medicinal Chemistry, School of Pharmacy for giving me teaching assistantship and opportunity to perform research work.

Table of Contents

List of Tables

Page

List of Figures

Page

Abstract

VITAMIN B_6 METABOLISM AND REGULATION OF PYRIDOXAL KINASE

By Amit K. Gandhi, Ph.D.

A dissertation submitted in partial fulfillment of the requirements for the degree of Doctor of Philosophy at Virginia Commonwealth University.

Virginia Commonwealth University, 2009

Major Director: Martin K. Safo, Ph.D
Assistant Professor, Department of Medicinal Chemistry

Pyridoxal 5'-phosphate (**PLP**) is the cofactor for over 140 vitamin B_6 (PLP)-dependent enzymes that are involved in various metabolic and biosynthetic pathways. Pyridoxal kinase (PL kinase) and pyridoxine 5'-phosphate oxidase (PNP oxidase) are the two key enzymes that metabolize nutritional forms of vitamin B_6, including pyridoxal (PL), pyridoxine (PN), and pyridoxamine (PM) to the active cofactor form, PLP. Disruption of the PLP metabolic pathway due to mutations in PNP oxidase or PL kinase result in PLP deficiency, which is implicated in several neurological pathologies. Several ingested compounds are also known to result in PLP deficiency with concomitant neurotoxic effects. How these mutations and compounds affect B_6 metabolism is not clearly understood. On the other hand, an emerging health problem is the intake of too

much vitamin B_6 as high doses of the reactive PLP in the cell exhibits toxic effects, including sensory and motor neuropathies. The overall aim of this research is to understand the catalytic function of PL kinase and the regulatory pathway of PLP metabolism.

Using site-directed mutagenesis (Asp235Asn, Asp235Ala), kinetic and structural studies, we have shown that Asp235 may play a catalytic role in PL kinase phosphorylation activity. We also show that human PL kinase binds its substrates, PL and MgATP synergistically, and that the enzyme requires Na^+ (or K^+) and Mg^{2+} for its activity. Using kinetic study, we show severe induced MgATP substrate inhibition of PL kinase in the presence of its product, PLP, and we postulate this to be due to the formation of a non-productive ternary complex (Enzyme•PLP•MgATP). Consistently, our crystal structure of human PL kinase (2.1 Å) co-crystallized with MgATP and PLP showed both MgATP and PLP trapped at the active site. Our hypothesis is that this abortive ternary complex might be a physiological process, and that PL kinase uses this mechanism to self-regulate its activity.

Our inhibition studies show theophylline, a bronchodilator as a mixed competitive inhibitor of human PL kinase with K_i of 71 μM. Our structural study (2.1 Å) shows theophylline bound at the substrate, PL binding site of human PL kinase. We also identified several potential PL kinase inhibitors from the DrugBank Chemical Compound database. Some of these compounds, including enprofylline, theobromine, caffeine, and lamotrigine, which incidentally exhibit similar neurotoxic effects as theophylline, show significant inhibitory effect on human PL kinase. Further studies are also planned to investigate the effect of these drugs on vitamin B_6 metabolism *in vivo*.

CHAPTER 1

General Introduction

1.1 Pathways of vitamin B_6 metabolism: There are six B_6 vitamers, including the primary forms pyridoxal (**PL**), pyridoxine (**PN**), and pyridoxamine (**PM**), and their phosphate derivatives **PLP**, **PNP**, and **PMP** (Figure 1). PLP, and to a lesser extent PMP, are the active cofactor forms that are used by various vitamin B_6 (PLP)- dependent enzymes for their activities.[1] Mammals cannot synthesize PLP *de novo* and use the dietary PN, PL and PM. Figure 2 shows the metabolic cycle of B_6 in mammals. This pathway involves PL kinase that phosphorylates PL, PN, and PM to PLP, PNP and PMP, respectively (rxn. 1, Figure 2). PNP and PMP are then converted to PLP by PNP oxidase (rxn. 2, Figure 2).[2, 3]

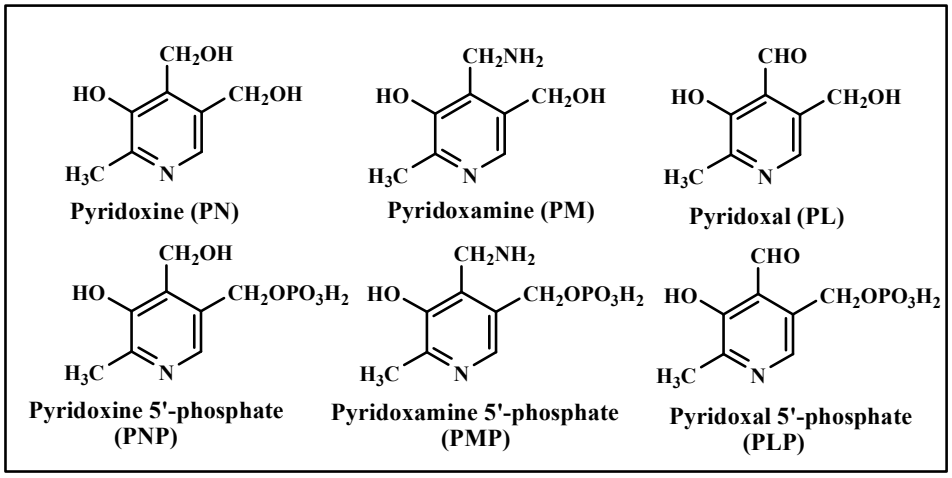

Figure 1: Structures of the six B_6 vitamers

In bacteria, plants and fungi this cycle exists in addition to a *de novo* biosynthetic pathway from common cellular metabolites. Another pathway for synthesizing PLP is the salvage pathway during protein degradation, where PMP, PNP and PLP are dephosphorylated by phosphatases to PM, PN and PL, followed by their conversion to PLP by the oxidase and/or kinase as shown in Figure 2. Several studies have shown that several phosphatases can perform this task and they have high turnover numbers.[4, 5, 6] The k_{cat} values of phosphatases are 30-fold higher than that of PL kinase and even several-fold greater than that of PNP oxidase.[6] The cellular content of PLP is thus dependent on PL kinase, PNP oxidase and phosphatases. PLP synthesized by PL kinase or PNP oxidase is used by several apo-B_6 enzymes as a cofactor to form the catalytically competent holo-enzymes (rxn. 3, Figure 2).[4, 5, 6] Both PL kinase and PNP oxidase are therefore key to supplying enough PLP to meet the requirement of the cell.

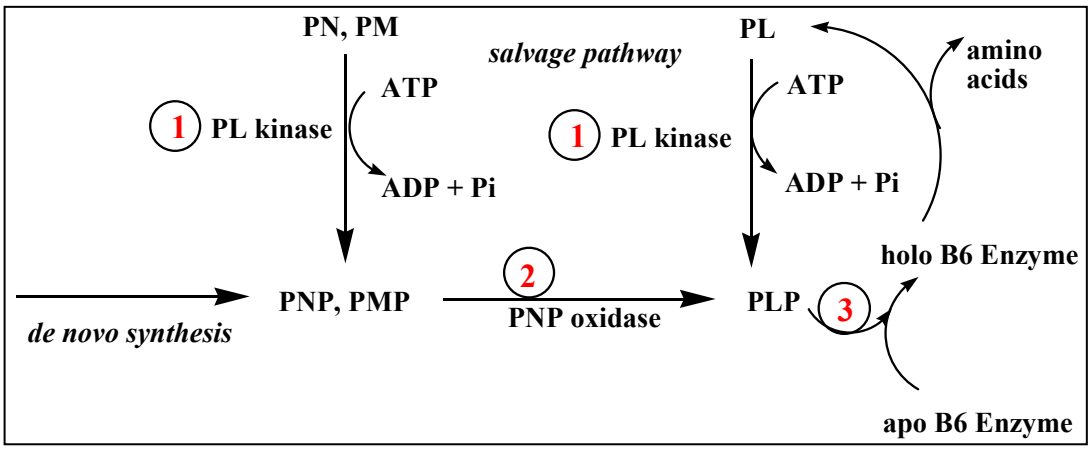

Figure 2: Scheme for the salvage pathway of vitamin B_6 metabolism

1.2 Structure and function of Pyridoxal Kinase: PL kinase catalyzes the addition of γ-phosphate of ATP to the 5' alcohol of PN, PM and PL and forms PNP, PMP and PLP, respectively (Figure 3).[4]

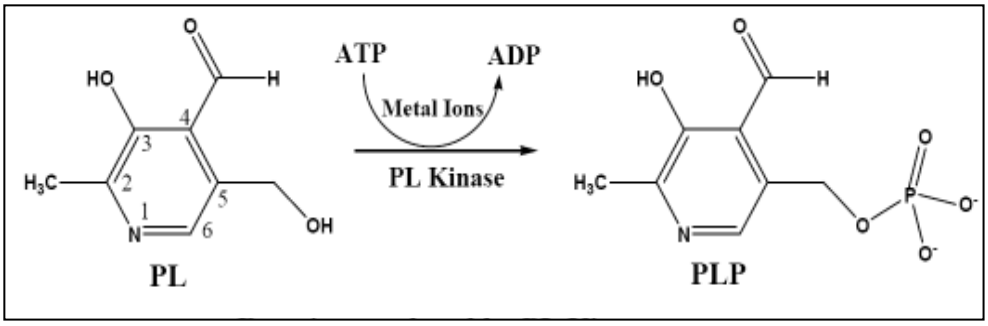

Figure 3: PL kinase catalyzed reaction

Currently the protein data bank lists amino acid sequences for over 100 close homologs of PL kinases from both prokaryotes and eukaryotes. The sequence identity ranges from 24-90 % to the human enzyme. Detailed sequence analysis of these PL kinase enzymes has been reported.[7, 8] A few of these enzymes have been studied to explore the substrate-binding site using inhibitors, chemical modification methods, spectroscopy and X-ray crystallography.[9-13] PL kinases have been purified from bacterial, plant and mammalian sources and evidence suggests that most eukaryote organisms contain a single PL kinase, coded by a *pdxK* gene. In contrast, prokaryotes contain two isoform PL kinases, encoded by *pdxK* and *pdxY* genes. The enzyme coded by the *pdxY* gene is not catalytically active, and subsequent mention of PL kinase is referred to the enzyme coded by the *pdxK* gene.[14, 15]

The crystal structures of *E. coli* PL kinase (ePL kinase) and sheep PL kinase (shPL kinase) have been elucidated, which show the enzyme to be a homodimer with one active site per monomer (Figure 4).[7-8, 11-12] All these kinases are members of the ribokinase superfamily as their crystal structures show the same typical ribokinase superfamily central core structure of β-sheets surrounded by α-helices, as well as conserved ATP and substrate binding site geometries. Unlike the prokaryotes, the eukaryote PL kinases are known to exhibit a relatively broad substrate specificity tolerating modifications at the 4'-position of vitamin B6. Structural studies of ePL kinase, and shPL kinase suggest that the different specificities may be due to differences in the active site structures.[7-8, 11-12]

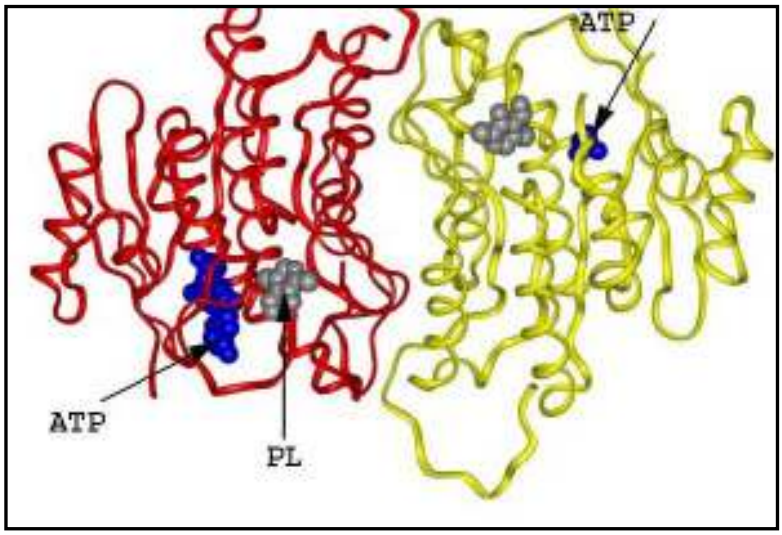

Figure 4: Homodimeric structure of ePL kinase with bound PL (grey) and ATP (blue).

1.3 Catalytic mechanism of Pyridoxal kinase: The phosphorylation mechanism has been elucidated for ePL kinase and shPL kinase, and follows a random sequential substrate addition. The enzyme requires the metal ion tandem, such as Mg^{2+} and K^{+} for activity. Asp235 is a conserved residue at the active site of PL Kinase. This residue is also

conserved in the ribokinase superfamily, and there is speculation that this residue serves as a base to deprotonate the substrate, PL prior to phosphorylation. [7-9, 16]

1.4 Pyridoxine 5'-phosphate oxidase: PNP oxidase catalyzes the terminal step in the synthesis of PLP by oxidizing the 4'-hydroxyl group of PNP or the 4'-amino group of PMP to an aldehyde, forming PLP with the transfer of 2 electrons to a tightly bound FMN, forming $FMNH_2$ (Figure 5). FMN is regenerated by transfer of the two electrons to oxygen forming hydrogen peroxide which is decomposed to water and oxygen by enzyme catalase. [4, 17-19]

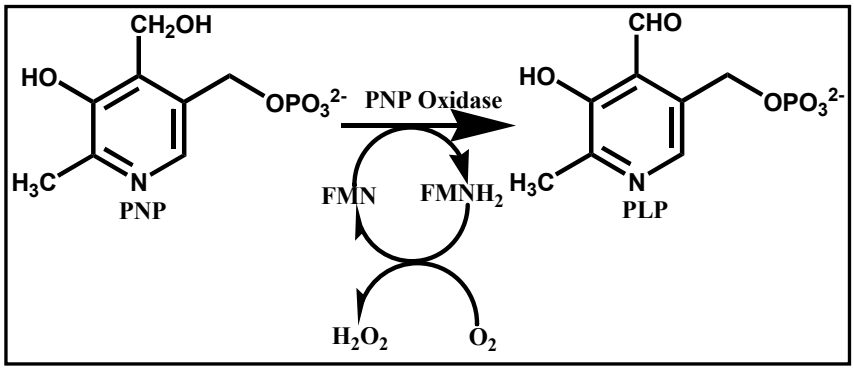

Figure 5: Reaction catalyzed by PNP oxidase

Structure of *E. coli* PNP oxidase (ePNP oxidase) in complex with FMN has been reported. This was the first enzyme in both the B_6 biosynthetic and salvage pathways for which a crystal structure was determined (Figure 6).[17] Later, ternary crystal structures of the human and *E. coli* PNP oxidase complexes with PLP (or PNP) and FMN in various active site conformations were also determined to gain insight into substrate binding and catalytic mechanism. Both human and *E. coli* enzymes have similar dimer folds, with each monomer containing FMN.[17-19]

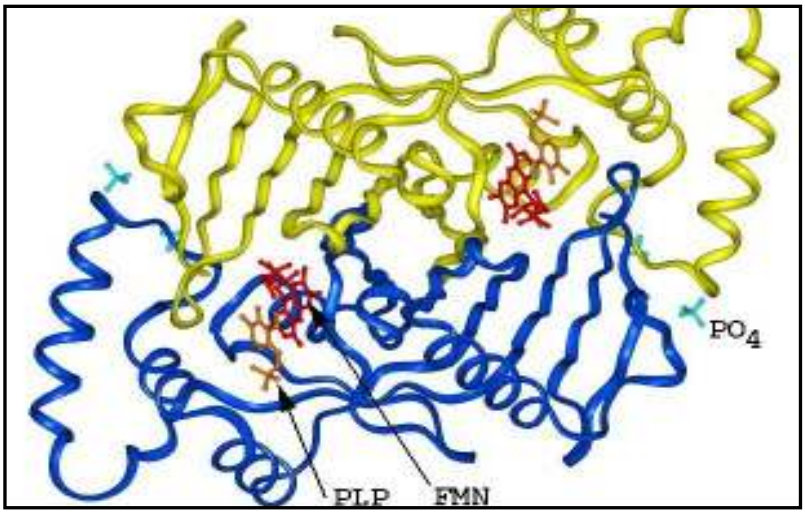

Figure 6: Homodimeric structure of ePNP oxidase with bound FMN (red) and PLP (brown).

1.5 Vitamin B_6 requiring enzymes: PLP is used by several apo-B_6 enzymes to form the catalytically active holo-enzymes. These enzymes are important in metabolic pathways involving carbohydrates, sphingolipids, amino acids, heme, and neurotransmitters.[20-24] The functional diversity of B_6 enzymes is illustrated by the fact that 145 distinct enzymatic activities noted by the Enzyme Commission (http://www.chem.qmul.ac.uk/iubmb/enzyme/) are PLP dependent, corresponding to ~4% of all classified activities. These enzymes are oxidoreductases, transferases, hydrolases, lyases and isomerases. The functions of many others are unknown.[24] The three dimensional structures of over 30 different PLP-dependent enzymes have been determined. In addition, the catalytic function, folding mechanism, as well as the substrate and reaction specificity of several of these enzymes have also been elucidated.[20, 24]

The PLP-dependent enzymes have been classified into at least 5 different fold-types based on amino acid sequence comparisons, predicted secondary structure elements and available three-dimensional structural information. Fold-type I is the largest family, and is further divided into at least 2 subclasses based on differences in conformation of the N-terminal part of the subunits. Some named examples of fold-type I enzymes are serine hydroxymethyltransferase (SHMT), glutamate decarboxylase (GAD), and aspartate aminotransferase (AAT). Examples of fold-type II are D-serine dehydratase and tryptophan synthase; examples of fold-type III are alanine racemase and eukaryotic ornithine decarboxylase; examples of fold-type IV are D-aminoacid aminotransferase and branched chain amino acid transferase; and an example of fold-type V is glycogen phosphorylase, the most abundant enzyme requiring PLP. PLP binds to these enzymes as an aldimine (Schiff-base) to an ε-amino group of lysine.[26, 27]

There is evidence to suggest that PLP synthesized by PL kinase or PNP oxidase is channeled to PLP-dependent enzymes.[28, 29] The Churchich group using fluorescence spectroscopy, affinity chromatography and a trapping agent (alkaline phosphatases) showed that PL kinase forms a complex with AAT (K_d of 3 μM), and that the trapping agent did not inhibit the transfer of PLP to the apo-B_6 enzyme.[28] A more recent study using fluorescence polarization and surface plasmon resonance (SPR) analyses showed that PL kinase can bind to AAT and GAD with dissociation constants of 4.9 μM and 2.7 μM, respectively.[29] Channeling would avoid PLP being destroyed by phosphatases or potentially interacting with other proteins because of the reactive PLP aldehyde moiety. This brings up an intriguing question as to how PL kinase and PNP oxidase, two

structurally different enzymes are able to recognize and interact with the over 140 B6-dependent enzymes that differ widely in their structural fold.

1.6 Vitamin B_6 enzymes, neurotransmitters and brain function: Figure 7 shows a partial list of neurotransmitters, whose synthesis requires PLP-dependent enzymes. **Pathway A:** GABA is the major inhibitory neurotransmitter in the mammalian CNS, and low levels are implicated with symptoms associated with epilepsy, convulsions, Parkinson's, Alzheimer's and Huntington's.[30-34] **Pathways B and C:** Dopamine, norepinephrine, epinephrine and serotonin have been implicated in Parkinson's disease and attention deficit hyperactivity disorder (ADHD).[35] **Pathway D:** D-serine serves as a co-agonist of the N-methyl D-aspartate receptor in mammalian brains, and its behavior is believed to be related to neurological disorders such as schizophrenia, Alzheimer's disease and amyotrophic lateral sclerosis.[36] **Pathway E:** Histamine, in addition to its role in hypersensitivity reactions, also plays an important role in memory.[37, 38]

PLP, PNP or PMP do not easily cross the blood–brain barrier, therefore they must be synthesized within brain tissues from the primary B_6 vitamers. Disruption of the salvage pathway could therefore lead to a decrease of PLP in the brain.[6] Because many B_6 enzymes in the brain compete for PLP, even a modest decrease in PLP availability could result in low levels of neurotransmitters with dire consequences on brain function. In a study by the Stover group, restriction of PN in MCF-7 cells led to a significant drop in cytosolic SHMT activity compared to mitochondrial SHMT.[39] This shows that PLP is not distributed equally among competing apo-B_6 enzymes. How this co-enzyme is made available to many apo-B_6 enzymes is therefore of profound interest.

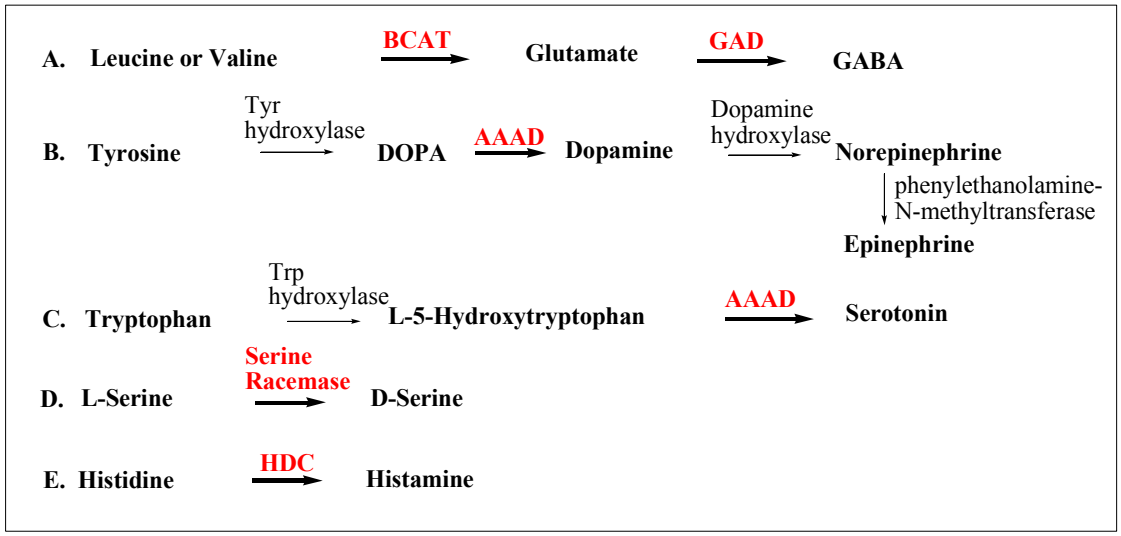

Figure 7: Synthesis of neurotransmitters by B_6 enzymes (colored red)

1.7 PLP and Vitamin B_6 toxicity: There are many potential toxic compounds in the cell, e.g. aldehydes, radicals, etc, that are part of metabolism. Cells have developed mechanisms to remove or keep their concentrations low. Aldehydes react with nucleophiles, especially amines, to form aldimines. Generally, aldehydes do not cause problems until raised to higher levels by an environmental insult or a genetic defect, e.g., advanced glycation end products implicated in diabetes due to sugar aldehydes reacting irreversibly with proteins.[40] PLP has been used often as a general Lys labeling reagent for proteins because of the high reactivity of the 4'-aldehyde. It is known that excessive doses of vitamin B_6 (> 200 mg/day) cause several health problems. The current recommended dietary allowance (RDA) for vitamin B_6 is 2 mg/day in the United States. Vitamin B_6 toxicity is known to damage sensory nerves, leading to numbness in the hands and feet, as well as difficulty in walking.[41-50] The sensory neuropathy is usually reversible when supplementation is stopped.[48] However, some patients are known to develop acute,

profound and permanent sensory neuropathy, and in some instances motor neuropathy and damage of the central nervous system.[46, 49, 50] High doses of B_6 are also found to induce convulsions in rats, which was suggested to be caused by formation of an aldimine between PLP and a lysine residue located in an extracellular loop of the GABA receptor.[41] In another study, PLP was observed to inhibit phenol sulfotransferase, a detoxification enzyme.[47] This begs the question as to how the cell regulates PLP to prevent toxic effects?

1.8 MgATP substrate inhibition of PL kinase in the presence of PLP: Accumulation of PLP in the cell as a free molecule must be kept low. PLP is a very reactive compound that forms aldimines with amino acids and Lys residues on proteins, and has been shown to result in toxic effects in humans and animal models.[41-50] Dephosphorylation of PLP is a well-known mechanism the cell uses to maintain low levels of free PLP.[6] Another proposed mechanism, which is presently not well understood, is regulation of PLP synthesis by PL kinase and/or PNP oxidase. In our previously published study with *E. coli* PL kinase, severe substrate inhibition of enzyme by MgATP in the presence of PNP or PLP was observed, suggesting possible feedback regulatory mechanism of PL kinase activity.[8]

1.9 Vitamin B_6 deficiency: A 2 mg/day RDA for Vitamin B_6 has been assumed to be adequate to maintain physiological plasma levels of B_6 at 20 nmol/L, however, a recent study has suggested that the RDA may be too low for some sections of the population due to the following: (i) inborn errors in PL kinase and/or PNP oxidase affecting the pathways of B_6 vitamer metabolism; (ii) drugs and other compounds that bind to PL kinase and inhibit its activities; (iii) drugs and other compounds that react with PLP and/or other B_6

vitamers and inactivate it; (iv) inborn errors that lead to accumulation of small molecules that react with PLP and/or other B_6 vitamers and inactivate it; (vi) renal dialysis, which leads to increased losses of B_6 vitamers; and (vii) inborn errors affecting specific PLP-dependent enzymes.[51, 52]

1.10 PL kinase inhibitors and PLP deficiency: Several drugs, as well as natural compounds are known to lead to PLP deficiency with concomitant neurotoxic effects.[53-61] Some of these compounds are known to inhibit PL kinase activity, which has been suggested to be the cause of the PLP deficiency.[53, 55, 59-61] Significant decreases in the serum concentration of PLP have been described in epileptic patients treated with anticonvulsant drugs (e.g., phenobarbital, phenytoin, carbamazepine, and valproic acid), which is reflected in reduction in the enzymatic activities of aspartate aminotransferase and alanine aminotransferase, two PLP-dependent enzymes.[62] Theophylline has been shown to significantly decrease plasma PLP levels in rabbits, asthmatic patients, or in healthy volunteers, resulting in peripheral neuropathy, seizures (acute overdose), sleeplessness, headache, restlessness, agitation, tremors and hallucinations.[54-58] A plasma concentration of theophylline greater than 110 μM is reported to be associated with these symptoms.[63] 4'-O-methylpyridoxine (an analog of vitamin B_6), found in Ginkgo biloba seeds leads to significant B_6 deficiency in mammals, resulting in convulsion, unconsciousness and other neuronal symptoms similar to that of theophylline.[64] This supplement is easily available over the counter and there is great concern over its unsupervised use.

Other drugs, including cycloserine and isoniazid, pyrazinoic acid, dopamine, penicillamine are also known to inhibit PL kinase resulting in many neurological side

effects (similar to those of theophylline).[53, 55, 59-61, 65] It is also known that a significant number of women using oral contraceptives who did not take B_6 supplements were found to be deficient in PLP.[52] Pyridoxine is usually prescribed to patients to prevent the associated neurotoxic side effects of some of these PL kinase inhibitors.[63, 65-69] Also, administration of vitamin B_6 to mice treated with theophylline is known to reduce the number of seizures; and in rabbits, vitamin B_6 reversed the changes in electroencephalograms caused by high doses of theophylline.[61, 65, 66] A recent study found that Roscovitine, an inhibitor of cyclin-dependent kinases, showed moderate inhibitory activity against PL kinase.[70, 71] Kinetic studies have been used to investigate the inhibitory effects of some of the above mentioned drugs.[55] There are several unanswered questions, including whether other compounds that exhibit theophylline neurotoxic effect could be doing so by inhibiting PL kinase activity. Also, it is not known how these PL kinase inhibitors affect B_6 pools in the cell.

1.11 Genetic defects in PL kinase or PNP oxidase and PLP deficiency: Human PL kinase and Human PNP oxidase genes are located on chromosomes 21q22.3 and 17q21.2, respectively. The autoimmune polyglandular disease type 1 has been linked to errors in chromosome 21q22.3. Patients show abnormal B_6 metabolism.[72] Four identified genetic defects in chromosome 17q21.2 result in mutations in the PNP oxidase enzyme, all of which reduce or completely abolish PNP oxidase activity leading to neonatal epileptic encephalopathy (**NEE**).[73-76] An example is a missense mutation (R229W) that leads to NEE. A recent study has elucidated the molecular basis of the reduced PNP oxidase R229W catalytic activity, which was found to be due to weak binding of the oxidase

cofactor, FMN, as well as the substrate, PNP. Based on their study, the investigators suggested that the use of riboflavin (vitamin B_2 or FMN) and pyridoxine, in conjunction with pyridoxal may offer some improvement over the current treatment protocol of PL or PLP alone due to the apparent loss of FMN from the PNP oxidase R229W variant.[77]

Several other studies have also reported strong association between other neurological disorders, including seizures, autism, attention deficit hyperactive disorder, Alzheimer's, Parkinson's, learning disability, anxiety disorders and PLP deficiency.[68, 75, 78-83] There has been considerable interest in treating the symptoms of some of the above disorders with vitamin B6, however, studies on the effect of B_6 supplementation show conflicting results. Consistently, administration of PN to patients with NEE failed, while PL/PLP offered some relief, supporting the location of the defect in PNP oxidase, as PL kinase is able to act on PL and convert it to PLP in the brain.[73, 75] Although, there is no direct evidence linking some of these neurological disorders to mutations in either the kinase or oxidase, these genes are clearly candidates for mutational analysis in affected patients. If such an error is identified, studies could be performed to investigate the role of the mutation in the enzymatic activity and the associated phenotypes. These studies could point to the correct pharmacologic intervention.

1.12 Other disorders associated with vitamin B_6 deficiency: Other non-neurological disorders are known to be caused, or have been suggested to be caused, by vitamin B_6 deficiency, including but not limited to the following - anemia, inability to maintain normal blood sugar levels, immune disorders and cardiovascular diseases. This is because PLP dependent enzymes are involved in heme synthesis, conversion of stored

carbohydrate to glucose to maintain normal blood sugar levels, homeostasis of homocysteine (a factor in cardiovascular diseases), and production of lymphocytes and interleukin-2.[76, 84-88]

1.13 Conclusion: PLP is used by several apo-B_6 enzymes as a co-factor to form the catalytically competent holo-enzymes serving vital roles in various transamination, decarboxylation, and synthesis pathways involving carbohydrates, sphingolipids, amino acids, heme and neurotransmitters. Thus vitamin B_6, in its active PLP form, supports more vital bodily functions than any other vitamin, yet little information is currently available on the mechanism of the regulation of PLP and vitamin B_6 metabolism, and how PLP is distributed among the dozens of competing apo-B_6 enzymes involved in neurotransmitter synthesis as well as other physiological functions.[20-24] On the other hand, disruption of the B_6 salvage pathway due to pathogenic mutations in PNPOx or PL Kinase or inhibition of these two enzymes or lack of nutritional intake of vitamin B_6 is known to result in PLP deficiency, which has been implicated in several pathologies including seizures, autism, Down's syndrome, schizophrenia, autoimmune polyglandular disease, Parkinson's, Alzheimer's, epilepsy, ADHD and learning disability.[73-76, 78, 89-91] Some drugs are also known to cause PLP deficiency by inhibiting PL kinase with concomitant neurotoxic effects.[53-61] It is likely that other drugs and natural products that cause similar side effects could also be inhibiting PL kinase.

Our goal is to understand the catalytic function of PL kinase and the regulatory pathway of vitamin B_6 metabolism. To achieve our goal the study was divided into four specific aims, including: (1) Determine the kinetic and structural properties of PL kinase;

(2) Determine the role of the active site residue Asp235 in PL kinase catalytic function; (3) Determine the method of kinetic regulation of PL kinase; and (4) Identify drugs and other compounds that are inhibitors of PL kinase.

CHAPTER 2

Determine the Kinetic and Structural Properties of Human PL Kinase

2.1 Introduction: PL kinases have been purified from bacterial, plant, and mammalian sources and evidence suggests that most eukaryote organisms contain a single PL kinase, coded by a *pdxK* gene. However, a large number of prokaryotes expressing PL kinases coded by both *pdxK* and *pdxY* genes have been reported.[7-8] While the enzyme coded by the *pdxY* gene is inactive, in the presence of MgATP, PL kinase coded by the *pdxK* gene catalyzes the addition of phosphate to the 5' alcohol of PN, PM and PL to form PNP, PMP and PLP, respectively and ADP.[4] The mechanism of phosphorylation has been elucidated for the sheep and *E. coli* PL kinase enzymes, and follows a random sequential substrate addition. [11-12]

Metals, both monovalent and divalent cations, are known to be absolute requirements for the mechanistic function of many PL kinases, providing driving forces for ATP binding and substrate catalysis. [7-8, 11-12] In *E. coli* PL kinase, the metal ion tandem Mg^{2+} and K^{+} are required for enzyme activity. In contrast, Zn^{2+} and K^{+} have been proposed

to be the physiological metals needed by both human PL kinase (hPL kinase) and sheep PL kinase for activity.[7-8, 11-12] However, a more recent study with the human enzyme clearly showed that under non-physiological substrate concentrations and/or at pH 6, where these previous assays were performed, Zn^{2+} does stimulate the activity, but under physiological conditions at pH 7.3, Mg^{2+} is the required divalent metal ion and Zn^{2+} inhibits the reaction.[92]

In order to understand the catalytic properties of hPL kinase and to characterize the role of the monovalent and divalent cations in the catalytic mechanism of hPL kinase, we expressed and purified hPL kinase and performed detailed kinetic and structural studies of hPL kinase.

2.2 Methods

2.2.1 Expression and purification of human PL kinase: Competent *E. coli* Rosetta (DE3)pLysS cells (Novagen) were transformed with a pET22b vector carrying the human *pdxK* gene insert. Transformants were grown in 6 L of Luria broth (LB) broth and after reaching an $O.D._{600nm}$ of 1.2 were induced with 0.5 mM Isopropyl β-D-1-thiogalactopyranoside (IPTG). Cells were grown for an additional 5 h at 30°C and harvested by centrifugation. The cell pellet was suspended in 200 mL of potassium phosphate buffer, pH 7.2, and ruptured by high pressure homogenization in an AVESTIN cell disrupter. Streptomycin sulfate was added to a final concentration of 10 g/L to remove excess nucleic acid. After an ammonium sulfate fractionation, and dialyzing the enzyme against 20 mM potassium phosphate buffer, pH 7.2, it was purified on

Trimethylaminoethyl (TMAE), phenyl sepharose, and hydroxyapatite columns.[92] The purity was >95%, as judged by SDS-PAGE.

2.2.2 Determination of kinetic constants of PL and MgATP: Human PL kinase enzyme used in the kinetic experiments were dissolved and dialyzed overnight against 20 mM sodium BES [N,N-bis(2-hydroxyethyl)-2-amino-ethanesulfonic acid] buffer, pH 7.2. All assays were performed at 37ºC in a 1-cm thermostated cuvette. Initial velocity studies for the conversion of PL to PLP were followed at 388nm in an Agilant 8454 spectrophotometer in 20 mM sodium BES buffer, pH 7.2. [9, 92] MgATP concentrations were varied between 200 μM and 1200 μM, and PL concentrations between 25 μM and 1 mM. Binding constants of PL and MgATP were determined by double reciprocal plots.

2.2.3 Human PL kinase activity in the presence of monovalent cations: Human PL kinase used in this kinetic experiment was extensively dialyzed against 20 mM triethanolamine BES, pH 7.2, prior to performing assays. All assays were performed in 20 mM triethanolamine BES, pH 7.2, and containing added monovalent salts from 0–50 mM at saturating ATP and PL concentration. All reagents used in the assays were dissolved in 20 mM triethanolamine BES, pH 7.2.[9]

2.2.4 Crystallization and structure determination of human PL kinase: Human PL kinase protein was dialyzed overnight against 20 mM K phosphate buffer (pH 7.0) containing 100 mM NaCl and then concentrated to 18 mg/mL (0.5 mM). Crystallization drops composed of 2 μL of protein solution and 2 μL of reservoir and equilibrated against 700 μL reservoir solution (100 mM Tris-HCl, pH 8.0, and 50% MPD) resulted in rectangular-shaped crystals. Crystallization of hPL kinase in the presence of 2 mM

MgATP was also attempted under similar conditions. The complex mixtures were first incubated on ice for about 3–4 hr before screening for crystallization.

For X-ray data collection, crystals were cryoprotected in solution containing 100 mM Tris-HCl buffer (pH 8.0) and 60% MPD with or without the MgATP before flash cooling in a cryogenic nitrogen stream. X-ray data were collected at 100 K using a Molecular Structure Corporation (MSC) X-Stream Cryogenic Crystal Cooler System and an R-Axis IV++ image plate detector, a Rigaku MicroMax–007 X-ray source equipped with MSC Varimax confocal optics operating at 40 kV and 20 mA. Crystals of hPL kinase in unliganded form diffracted to 2.0 Å The hPL kinase grown in the presence of MgATP diffracted to 2.2 Å. The data sets were processed with the MSC d*TREK software program. The Matthews Coefficient of 3.2 and water content of 61% are consistent with one dimer per asymmetric unit.

The crystal structure of the unliganded hPL kinase was solved using the Web-tool CaspR, which executes an optimized molecular replacement procedure.[93] The hPL kinase sequence and the search models of shPL kinase (PDB code 1LHP; 87% sequence identity to human PL kinase) and ePL kinase (PDB code 2DDM; 24% identity) were first used to derive multiple structure-sequence alignments with the program T-Coffee,[94] followed by homology model building with the program MODELLER.[95] Fifteen models were generated with different spatial conformations, and each was automatically screened in CNS. [97] Two of the models had the best convergence, with correlation coefficients of about 0.66 and *R*-factors of 0.40. The next best solution had a correlation coefficient of 0.40 and an *R*-factor of 0.53.

The model from the converged solution was used for subsequent structure refinement, by means of CNS, with a bulk solvent correction. The starting model was subjected to rigid body, positional, and simulated annealing refinements with all 2.0 Å crystallographic data to R_{work}/R_{free} of 33.5% / 38.5%. Some residues were omitted due to weak densities. The model was subsequently adjusted, followed by further cycles of refinements and addition of Na^{+}, PO_4^{2-}, MPD, and water molecules.

The partially refined hPL kinase structure without solvent molecules and metal ions was used as the starting model to refine against the diffraction data from the cocrystals of hPL kinase and MgATP. Initial rigid body, positional, and simulated annealing refinements at 2.2 Å resolution to R_{work}/R_{free} of 26.2% / 32.2% clearly showed ATP, Mg^{2+} and Na^{+} bound at the active site of the complex, which were modeled in the structure. The refinement statistics are summarized in Table 1. Atomic coordinates and structure factors have been deposited in the RCSB Protein Data Bank with the accession codes 2YXT and 2YXU for the unliganded and MgATP-bound hPL kinase, respectively. [9]

Table 1. Data collection and refinement statistics for the hPL kinase crystals.

	Unliganded	MgATP
Data collection		
Space group	I222	I222
Unit cell *a*, *b*, *c* (Å)	90.63, 115.29, 172.40	90.46, 115.12, 170.20
Resolution (Å)[a]	30 - 2.0(2.07 - 2.00)	30 – 2.2 (2.28 – 2.20)
Unique reflections	60825(6055)	44337 (4270)
Mean redundancy	4.7(4.5)	6.7(6.6)
Completeness (%)	99.3(99.9)	97.6(95.9)
Average I / σ(I)	11.9(4.4)	14.5(5.2)
R_{merge}[b]	0.073(0.340)	0.082(0.366)
Refinement statistics		
R_{work} (95% data)[c]	0.206(0.448)	0.192(0.388)
R_{free} (5% data)[d]	0.245(0.473)	0.243(0.415)
Average B (Å^2) / No. of non-H atoms		
Protein	38.6 / 4797	38.5 / 4842
Water	52.2 / 518	53.0 / 474
MPD	69.6 / 112	68.8 / 96
Anion (PO_4^{2-})	97.9 / 30	97.7 / 25
Cation (Na^+, Mg^{2+})	62.3 / 2	26.6 / 4
ATP		34.0 / 62

[a]Numbers in parentheses refer to the outer (highest) resolution shell.

[b]$R_{merge} = \sum|I - \langle I \rangle| / \sum(I)$, where I is the observed intensity and $\langle I \rangle$ is the weighted mean of the reflection intensity.

[c]$R_{work} = \sum||F_o| - F_c|| / \sum|F_o|$, where F_o and F_c are the observed and calculated structure factor amplitudes, respectively.

[d]R_{free} is the crystallographic R_{work} calculated with 5 % of the data that were excluded from the structure refinement.

2.3 Results and Discussion

2.3.1 Kinetic constants and synergism between PL and ATP: Using pig brain extracts of PL kinase, Churchich and Wu first showed that the phosphorylation reaction catalyzed by PL kinase with MgATP result in significant amounts of the binary complexes of enzyme-ATP and enzyme-pyridoxal.[13] Recent kinetic and structural studies with sheep, human and E. coli enzymes are consistent with this random sequential substrate addition mechanism.[7-8, 11-12, 92] The question we ask is whether there is any synergism in the binding of ATP and PL. If MgATP and PL bind randomly, and binding of one substrate changes the binding constant for the other substrate by a factor α, the hPL kinase system can be described by the equilibria shown below (Figure 8).[98]

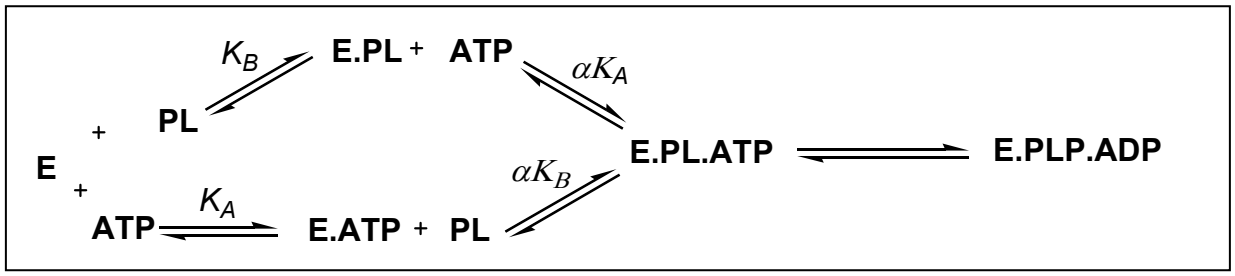

Figure 8: Binding equilibria for human PL kinase substrates

The complexes E.ATP, E.PL, E.PL.ATP, and E.PLP.ADP are transitory complexes. K_A and αK_A are binding constants for ATP in the absence of PL and infinite PL, respectively. K_B, and αK_B are binding constants for PL in the absence of ATP and infinite ATP, respectively. The binding constants were determined from double reciprocal plots of initial rates with PL and MgATP as the variable and fixed substrates. In general, each

substrate was varied over a 10-fold concentration range. The pattern of lines in the double-reciprocal plots crossed at a point above the negative x axis when either ATP or PL was the variable substrate (Figures 9 and 10). The 1/initial rate versus 1/[ATP] plot at different fixed concentration of PL or vice versa were drawn to calculate the values of K_A and K_B, respectively.

Apparent initial rate values, calculated from plots of 1/intial rate versus 1/[PL] at different fixed concentration of ATP, were plotted against the corresponding 1/[ATP] to determine αK_A (Figure 11). Similarly, apparent initial rate values, calculated from plots of 1/intial rate versus 1/[ATP] at different fixed concentration of PL, were plotted against the corresponding 1/[PL] to determine αK_B (Figure 12). Values of K_A, K_B, αK_A, and αK_B are shown in Table 2. The factor α which describes synergistic behavior between the substrates is ~0.31, and is calculated using the equation 1.

$\alpha = [\alpha K_A] / [K_A]$ or $\alpha = [\alpha K_B] / [K_B]$ ---------- **Equation 1**

Since α is less than unity, it indicates binding of ATP increases the affinity of human PL kinase for the PL or vice versa.[98]

Table 2: Kinetic parameters of human PL kinase substrates (in μM)

K_A	K_B	αK_A	αK_B
833	95	266	30.5

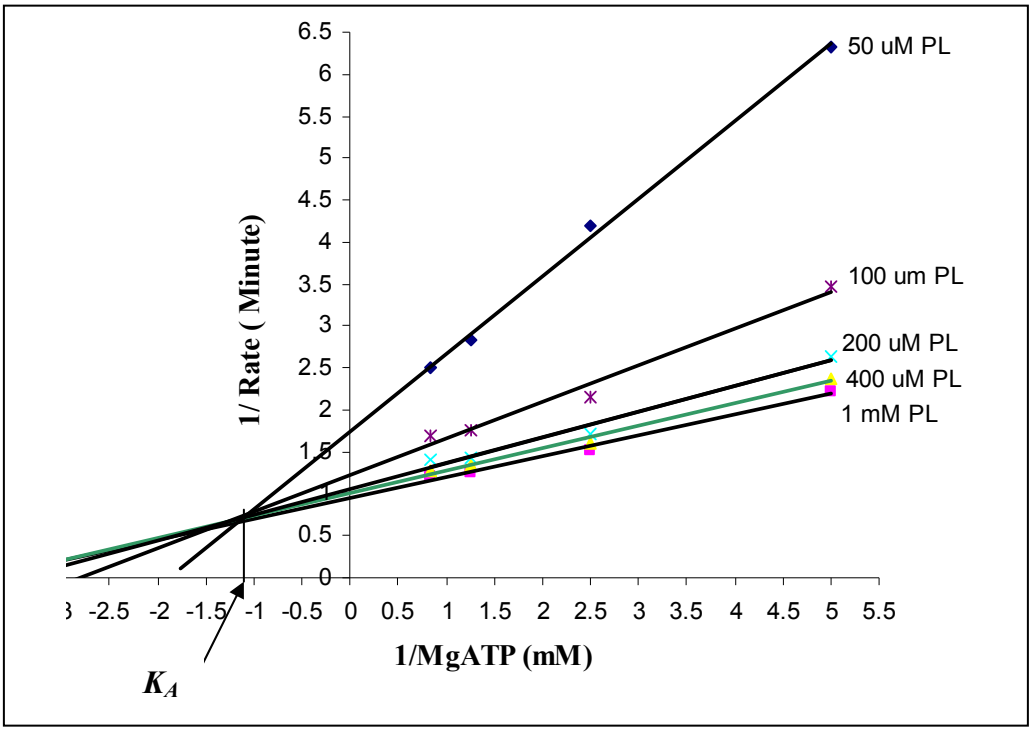

Figure 9: Determination of K_A

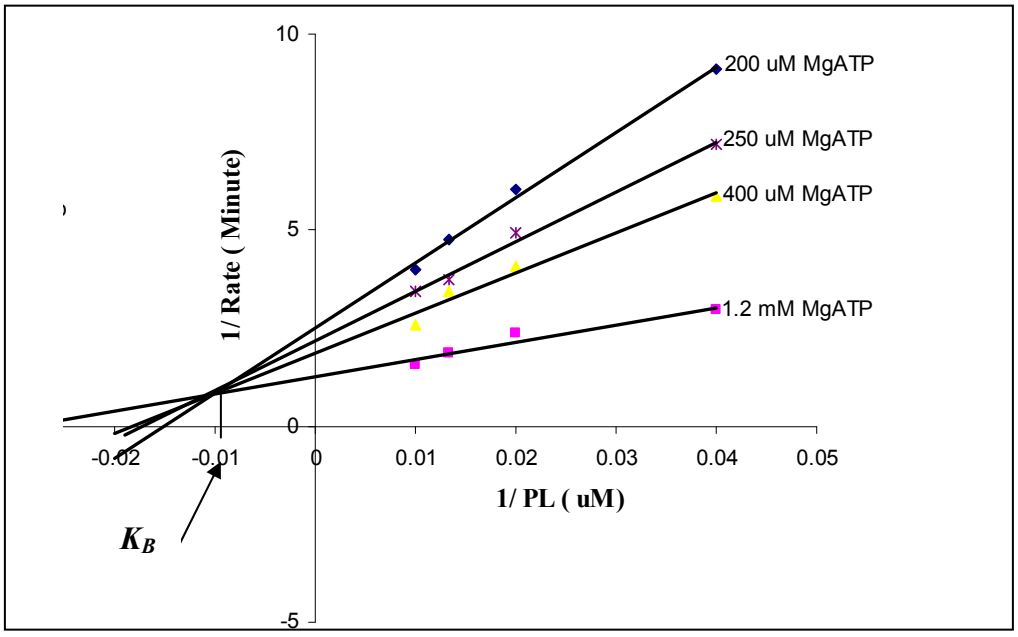

Figure 10: Determination of K_B

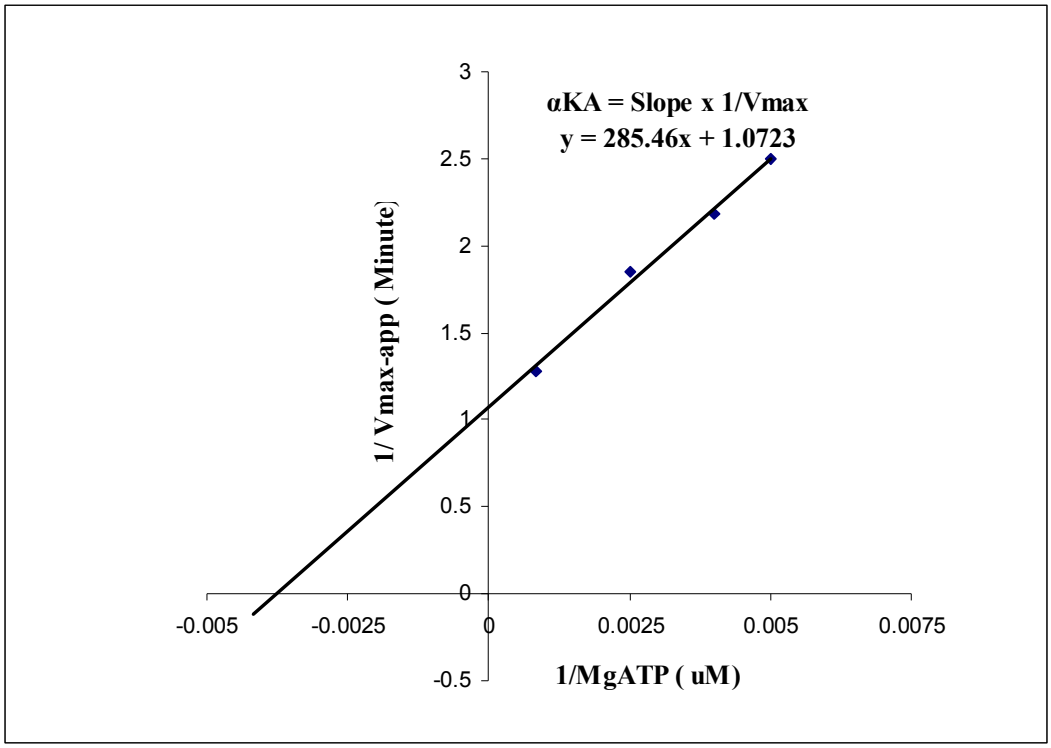

Figure 11: Determination of αK_A

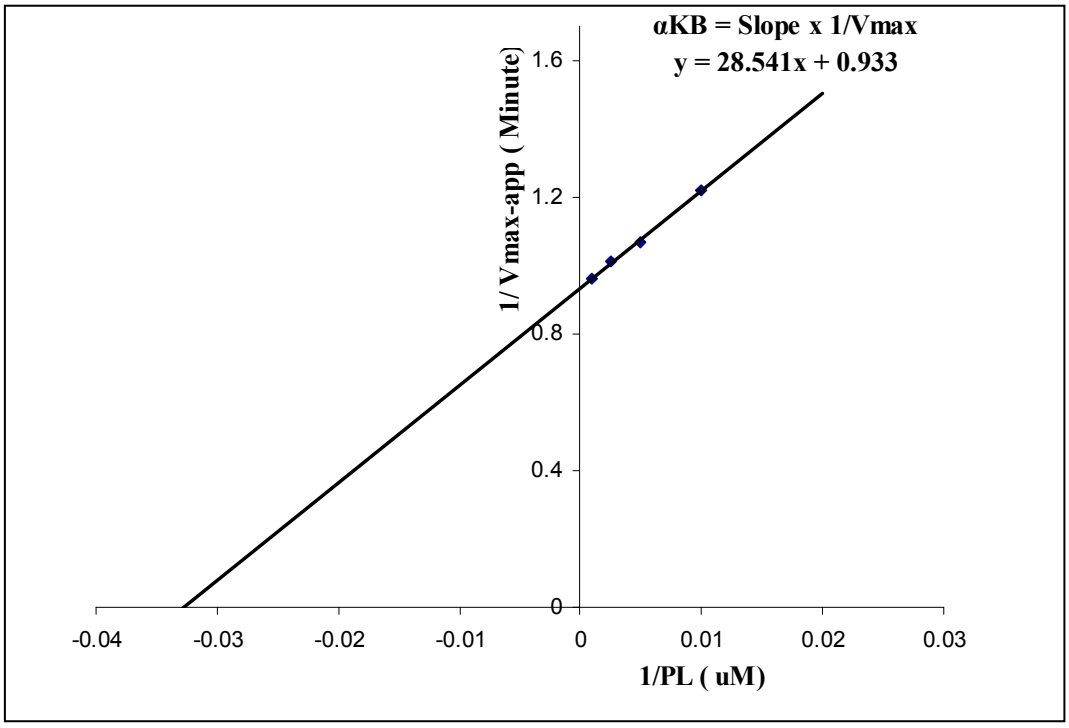

Figure 12: Determination of αK_B

2.3.2 Effect of different monovalent metals on human PL kinase activity*:* We measured enzyme activity using a variety of monovalent cations under saturating PL and MgATP concentrations, and found that both Na^+ and K^+ activated the hPL kinase while other monovalent cations, Li^+, Cs^+, and Rb^+ do not show significant activity (Figure 13).[9]

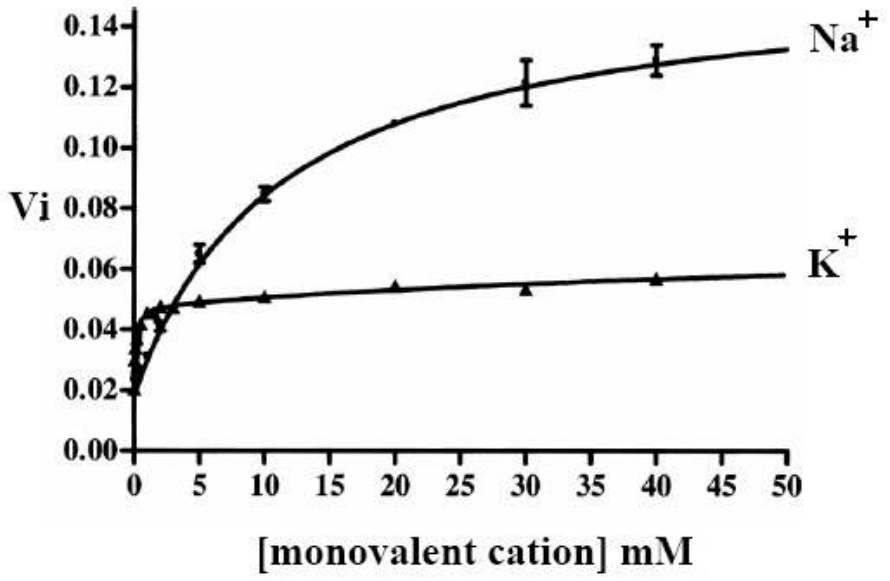

Figure 13: Activity of human PL kinase in the presence of either Na^+ or K^+.
(Closed circles for Na^+ & triangles for K^+).

2.3.3 Structural Studies - Crystal structures of human PL kinase, as well as its complex with MgATP were determined at resolutions of 2.0 Å and 2.2 Å, respectively, to understand the kinetic properties of PL kinase on molecular level. The two crystals are isomorphous, and both belong to the orthorhombic space group I222. The asymmetric unit of both structures contains monomers A and B, which are related by a noncrystallographic dyad axis. Each monomer of hPL kinase consists of nine α-helices and 11 β-strands (Figure 14A).

The unliganded shPL kinase, and ePL kinase crystal structures have been reported at ~ 2.1 Å resolution, while the corresponding MgATP complexes of shPL kinase and ePL kinase have also been reported at 2.6 Å resolution. All these PL kinase structures show the same typical ribokinase superfamily central core of β-sheets surrounded by α-helices, as well as similar dimeric assembly.[7-8, 11-12] A structure of the hPL kinase dimer is shown in Figure 14B. The overall structures of hPL kinase and hPL kinase-MgATP are very similar. The dimers (for 577 Cα pair atoms) or monomers (for 299 Cα pair atoms) superimpose on each other with an RMSD of 0.37 Å, which compares with ~0.35 Å between monomers within each structure. This indicates that binding of ATP at the active site does not induce larger conformational changes than exists between two monomers within the same crystal. Similar observations were also reported for the ePL kinase and shPL kinase structures.[7-8, 11-12]

In the unliganded hPL kinase crystal, we observed bound Na^+ in both active sites, close to where the ATP γ-phosphate group is located in the hPL kinase–MgATP complex (Figure 15). The Na^+ is penta-coordinated with water molecules (average distance of 2.1 Å). The water molecules are in turn hydrogen-bonded to the side chains of Asp113, Glu153, and Thr186, as well as the amide nitrogen and oxygen atoms of Asn150 and Thr148, respectively (Fig. 15A). The unliganded hPL kinase model also contains 14 MPD molecules, located in the active sites, on the surface of the protein at various crevices, as well as the interfaces of crystal contacts. Interestingly, three MPD molecules span across the PL (MPD 3) and ATP (MPD 1 and MPD 2) binding cavities in each of the monomers of hPL kinase, mimicking the substrate molecules (Fig. 15B).

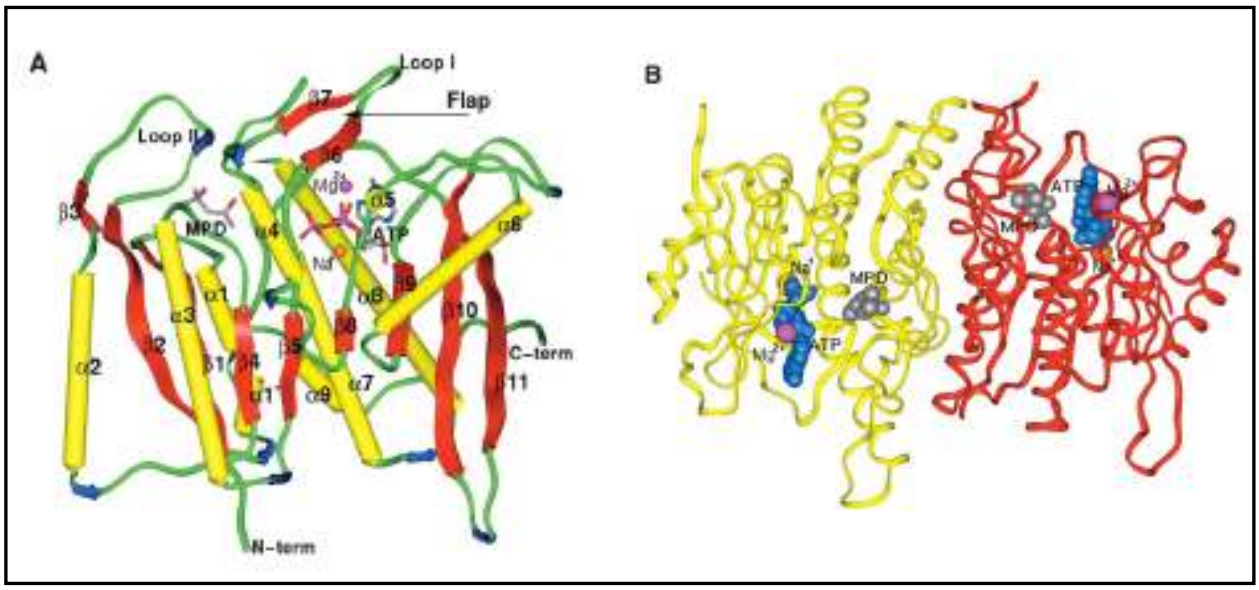

Figure 14: Overall structure of hPL kinase. (*A*) The monomeric structure with bound ATP (stick), MPD (stick), Na^+ (brown sphere), and Mg^{2+} (magenta sphere) at the active site. α-Helices and β-strands are colored yellow and red, respectively. The secondary structures are labeled. (*B*) The dimeric structure, also with bound ATP (cyan CPK), MPD (gray CPK), Na^+ (brown sphere), and Mg^{2+} (magenta sphere). Monomers A and B are colored red and yellow, respectively.

Each of the two active sites in the liganded hPL kinase–MgATP complex binds ATP, Mg^{2+}, and Na^+ molecules. The ATP γ-phosphate group and the two metal ions, Na and Mg are remarkably well defined in both active sites (Figures 16C,D). Comparison of hPL kinase and hPL kinase–MgATP structures shows that residues 224–228, which form part of the loop region between strand β11 and helix α7 have rotated away from the active site to allow binding of the ATP adenine (Figure 15B). Additionally, the active site structure formed by the strand β6-Loop I–strand β7, which is referred to as a flap in PL kinases, has moved closer to the bound ATP (Figure 15B). The mode of ATP–protein interaction is depicted in Figure 16A, which is similar to those described for shPL kinase and ePL kinase.[7-8, 11-12] Of note is that all the residues that make contact with the β-/γ-

phosphate groups are totally conserved in PL kinases.[7-8, 11-12] Binding of ATP has also displaced two MPD molecules (MPD 1 and MPD 2 in Figure 15B) observed at the ATP binding site in the unliganded structure. Like the unliganded structure, we still observed a MPD molecule bound at the PL binding site (MPD 3 in Figure 15B).

The Mg^{2+} in hPL kinase is located between the ATP α- and β-phosphate groups and it's octahedrally coordinated (Figures 15C) - two ligands from the ATP α/β-phosphate groups (~2.1 Å), a ligand each from the carboxyl oxygen of Asp118 (~2.2 Å) and the hydroxyl of MPD (~2.3 Å), and two water molecules (~2.2 Å). The high charge density of Mg^{2+} is thus balanced by the negatively charged carboxyl and phosphoryl groups, and most importantly, the Mg^{2+} location is consistent with its function by binding to the bis-phosphate moiety to neutralize the negative charges and stabilize the ADP leaving group during the phosphorylation reaction.

Binding of ATP has displaced the bound Na^{+} in the unliganded hPL kinase by ~2.0 Å to another position (Figure 16B). Unlike the unliganded structure, the Na^{+} in the complex now makes direct bond contacts with the protein and the ATP (Figure 16C). The coordination of the Na^{+} in hPL kinase-MgATP appears to be trigonal–bipyramidal or square–pyramidal (Figure 16C), with two donor atoms from the ATP γ-phosphates group (~2.5 Å), one donor atom from the amide oxygen of Thr148 (~2.4 Å), and one donor atom from the hydroxyl of Thr186 (~2.3 Å), and a water molecule (2.3 Å). Our studies with the monovalent cations show that Na^{+} and K^{+} activated the enzyme significantly with the former showing more activation. In the structural studies of sheep PL kinase, K^{+} instead of Na^{+} was used to crystallize the sheep enzyme.[11-12] Comparison of the sheep and our human

PL kinase structures show K^+ and Na^+ positions overlap (Figures 16B). Nevertheless, while Na^+ has a five-coordination shell in the human enzyme, K^+ in the sheep enzyme is octahedrally coordinated with the protein residues Thr186, Asp113, Glu153, and Thr148, as well as the ATP β-phosphate group and a water molecule. Thus, when K^+ is replaced by Na^+ in the human enzyme only the interactions with Thr148 and Thr186 are conserved, and contributions from Asp113 and Glu153 are lost. In both structures, the two metal ions, through their direct interaction with the protein and ATP phosphate groups, should be able to engage and anchor the ATP for catalysis.

The question remains as to why the human enzyme is more active in the presence of Na^+ than K^+. It is possible that replacement of K^+ with Na^+ changes the geometry of the active site to a more optimal orientation of catalytic residues, leading to greater enzyme activity in the presence of the later cation. This is consistent with several studies that suggest that coordination sphere of metal cations plays a significant role in enzyme activity.[99-102] In dialkylglycine decarboxylase, replacement of Na^+ with K^+ is known to drastically change the geometry of coordination and perturbs residues that control binding of substrate.[99-100] In thrombin, changes in coordination sphere of Na^+ and K^+ is known to affect the oxyanion hole geometry explaining the differences in kinetic activity.[101] In some proteins, however, replacement of one metal with another, such as K^+ with Na^+ in pyruvate kinase, results in no structural change even though the enzyme is inactive in the absence of K^+.[102]

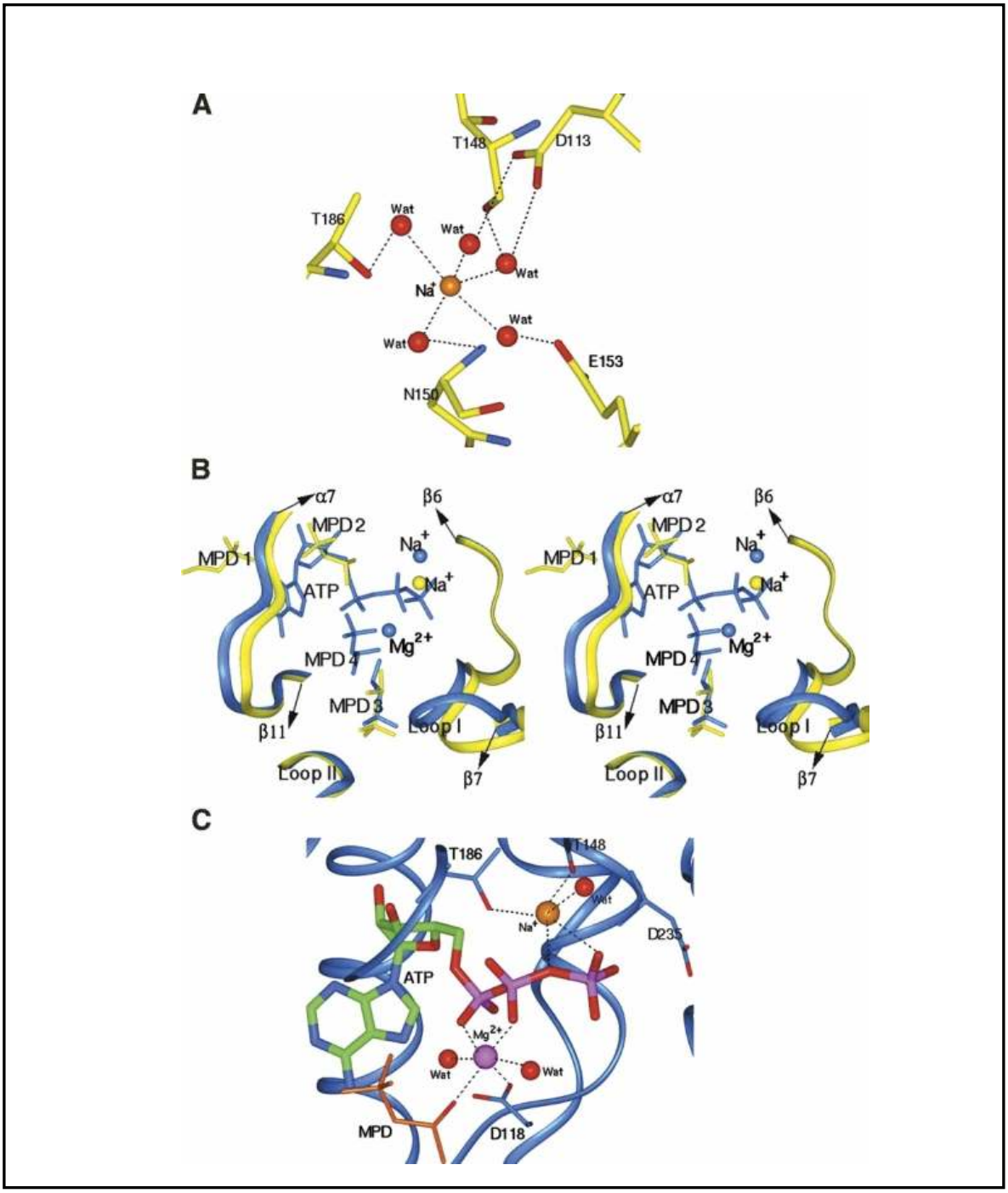

Figure 15: Structural basis of monovalent and divalent ions' activation of hPL kinase. (*A*) Na^+ (brown sphere) bound to the active site of monomer A of unliganded hPL kinase. (*B*) Stereoview of the superimposed active sites of unliganded hPL kinase (colored yellow) and hPL kinase-MgATP complex (colored cyan). Three MPD molecules occupy the active site of the unliganded hPL kinase structure, whereas two are found in the hPL kinase–MgATP complex. (*C*) Na^+ (brown sphere) and Mg^{2+} (magenta sphere) binding modes at the active site of hPL kinase–MgATP complex

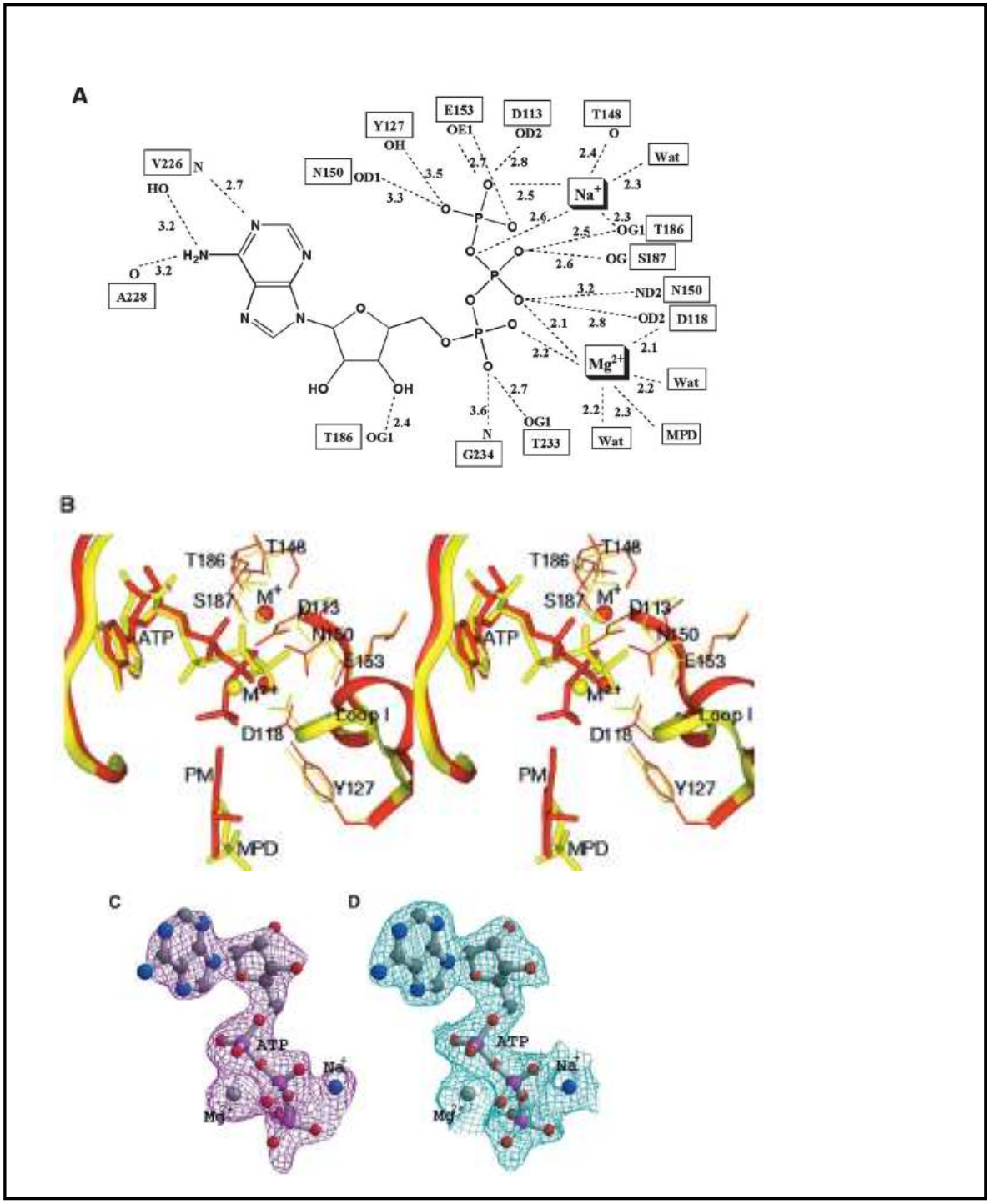

Figure 16: The active site and substrate of hPL kinase–MgATP complex. (*A*) Schematic diagram showing interactions between Na^{+}, Mg^{2+}, ATP, and the protein residues of hPL kinase.(*B*) Stereoview of the superimposed active sites of hPL kinase–MgATP (colored yellow) and shPL kinase–MgATP (colored red). (*C*) A Fo−Fc map (contoured at the 3.0 σ level) of Na^{+}, Mg^{2+}, and ATP of the hPL kinase–MgATP complex, calculated before the metal ions and ATP were added to the refined model. (*D*) A 2Fo−Fc map (contoured at the 1.0 σ level) of Na^{+}, Mg^{2+}, and ATP of the hPL kinase–MgATP complex. Both maps are superimposed with the final refined models.

It should be recalled that in unliganded hPL kinase, there is a bound Na^+, which is penta- or tetra- coordinated with solvent molecules (Figure 15A), however binding of ATP displaces the Na^+ to another position, closer to the protein, where it makes direct interaction with the protein in addition to the ATP (Figure 15B and C). Note that the B-values of the Na^+ ions in the unliganded crystal (~60 $Å^2$) are much higher than those in the MgATP complex (~30 $Å^2$), suggesting stable binding with the mediating waters excluded. It's known that substrate binding to a stabilized enzyme-M^+ complex is more favorable as the entropic penalty of ordering the enzyme to form the enzyme-substrate complex is offset by the previously bound M^+.[103] This is consistent with the observed increased affinity for ATP in the kinases. Nevertheless, due to the small size of Na^+ (0.9 Å), it should form a relatively strong interaction with 4 or 5 solvent molecules, while the larger K^+ (1.33 Å) should prefer more solvent molecules with relatively weaker interactions. The ability to strip off water molecules from the hydration sphere should therefore be easier with K^+ than with Na^+, and could explain why the enzyme shows greater affinity for ATP in the presence of K^+ than Na^+.[104-106]

A known K^+ position in the *E. coli* enzyme would help throw light on the structural basis of the M^+ selectivity in ePL kinase. However, it seems that human and perhaps other eukaryote PL kinases have evolved K^+ selectivity by imposing 6-coordinate geometric constraint on the coordination sphere that may not be accessible by Na^+. In some ribokinase superfamily enzymes, the monovalent cation does not make contact with the protein but only with the ATP, and it's believed that the cation exerts its influence indirectly by perturbing the conformation of the active site residues.[107-108] On the other

hand, in some PLP-dependent enzymes, such as serine hydratase,[109] tryptophanase[110], the M^+ does not make contact with the substrate, but aids to organize the architecture of the active site for catalysis.[109]A recent mini review article elegantly classified the enzymes that have a monovalent cation bound to ATP and the protein residues as M^+-activated Type I, while those that bind only to either the protein or the substrate as M^+-activated Type II.[103] PL kinases obviously belong to the former, while other non-PL kinase members in the ribokinase superfamily of proteins, such aminoimidazole riboside kinase[107] belong to the latter. Thus the binding mode of monovalent cations may be an indicator as to how these species have evolved from each other.

2.4 Conclusion

Pyridoxal kinase catalyzes the transfer of a phosphate group from ATP to the 5′ alcohol of pyridoxine, pyridoxamine, and pyridoxal. In this work, we report kinetic constants for hPL kinase substrates, PL and ATP and kinetic studies were conducted to examine monovalent cation dependence of hPL kinase kinetic parameters. The kinetic study suggests synergistic binding of Mg-ATP and PL, which could be important in the regulation of PL kinase activity. We have also determined the crystal structure of hPL kinase in the unliganded form, and in complex with MgATP to elucidate the molecular basis of monovalent and divalent ions activation of the enzyme.[9] The crystal structure reveals Mg^{2+} and Na^+ acting in tandem to anchor the ATP at the active site. The structure also suggests that differences in PL kinase activity in the presence of different monovalent ions could be due to differences in the coordination sphere of the ions. It is quite possible

that under physiological conditions in the cells, where K^+ is several fold higher than Na^+, the enzyme will be in its K^+ form.

CHAPTER 3

Determine the Role of the Active Site Residue Asp235 in PL Kinase Catalytic Function

3.1 Introduction: The crystal structures of *Escherichia coli*, sheep and human PL kinases reveal a functional dimeric structure, with one active site per each monomer. PL kinases are classified as members of the ribokinase superfamily, since they show the same typical central core tertiary structures of β-sheets surrounded by α-helices, as well as conserved ATP and substrate binding site geometries.[7-9, 11-12] Members of this enzyme superfamily catalyze the phosphorylation of the C5′-hydroxyl group of their respective substrates using ATP. In PL kinases and in the ribokinase superfamily as a whole, a conserved Asp235 residue is observed to make a hydrogen-bond interaction with the C5′-OH group of the substrates, and the current working hypothesis suggests this residue to be the base that deprotonates the C5′-OH group, with the resulting negatively charged O5′ atom making a direct nucleophillic attack on the ATP γ-phosphate (Figure 17).[7-9, 11-12]

In this study, three site-directed mutant forms of human PL kinase, including D235H, D235A and D235N were constructed, however only the latter two could be expressed and purified. Kinetic and structural studies were carried out to determine if Asp235 plays a catalytic role in PL kinase enzymatic activity.

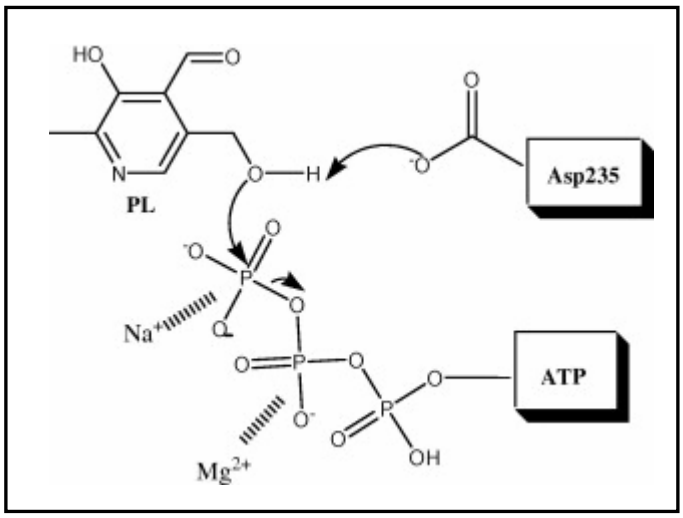

Figure 17: Proposed reaction mechanism by PL kinase.

3.2 Methods

3.2.1 Site-directed mutagenesis and purification of enzymes: The D235A and D235N mutants were made on the wild-type construct pET22b(+) carrying the human *pdx*K gene insert[91] using the QuickChange™ Site-Directed Mutagenesis Kit from Stratagene (La Jolla, CA). The mutations were confirmed by sequencing the cDNA inserts. The mutated and wild type gene inserts were then transferred into a pET28a(+) vector by use of NdeI and XhoI unique restriction sites, and then transformed into *E. coli* Rosetta (λDE3) pLysS competent cells for protein expression (Novagen).

The Rosetta cells with the wild type and mutated genes were grown in 6L of LB-kanamycin–chloramphenicol medium to an optimal density of 1.2 at 600 nm, and then induced with 0.5 mM IPTG. Cells were grown for an additional 5 h at 32 °C and harvested by centrifugation. The cell pellets were resuspended in 250 ml of 50 mM sodium

phosphate buffer, pH 8.0, and disrupted by high pressure homogenization in an AVESTIN cell disrupter. Streptomycin sulfate was added to a final concentration of 10 g/L to remove excess nucleic acids. The enzyme was dialyzed in 50 mM sodium phosphate buffer, pH 8.0, and then purified using a Ni-NTA (Nickel-nitrilotriacetic acid) column. Fractions containing 95% purity, as judged by SDS-PAGE were pooled and concentrated.[16]

3.2.2 Determination of kinetic constants: Wild-type, and D235A and D235N mutants used in the kinetic experiments were dialyzed overnight against 20 mM sodium BES buffer, pH 7.2. Kinetic assays were performed at 37 °C in a 1 cm thermostated cuvette. Initial velocity studies for the conversion of PL to PLP were followed at 388 nm in an Agilant 8454 spectrophotometer in 20 mM sodium BES buffer, pH 7.2.[9, 92] MgATP concentrations were varied between 100 to 800 μM, and PL concentrations between 20 to 300 μM. The K_m and k_{cat} values for PL and MgATP were determined by double reciprocal plots.

3.2.3 Crystallization, data collection and structure determination: The D235A mutant was co-crystallized with PL and ATP, while D235N mutant was co-crystallized with ATP. Crystallization drops were composed of 2.5 μL of protein solution (with 2.5 mM MgATP and/or 1 mM PL) and 2.5 μL of reservoir and equilibrated against 700 μL reservoir solution (100 mM Tris–HCl, pH 8.0, and 57% MPD, 5 mM $MgSO_4$).

Crystals were cryoprotected in solution containing 100 mM Tris–HCl buffer (pH 8.0) and 60% MPD with the appropriate substrates before flash cooling. X-ray data were collected at 100 K using a Molecular Structure Corporation (MSC) X-Stream Cryogenic Crystal Cooler System and an R-Axis IV++ image plate detector, a Rigaku MicroMax–

007 X-ray source equipped with MSC Varimax confocal optics operating at 40 kV and 20 mA.

The isomorphous human PL kinase structure (PDB code 2YXT)[9], mutating Asp235 to Gly, and omitting bound ATP, phosphate, water and MPD molecules was used as the starting model for the refinements of the two mutant structures. All refinements were performed with the CNS program.[97]

After rigid body refinement, conjugate gradient minimization and simulated annealing using the diffraction data of D235A, difference density at residue 235 suggested an Ala consistent with nucleotide sequencing result. Densities were also identified for ATP, Mg^{2+} and Na^{+} in both active sites. We also observed bound PLP and PL molecules in the active site of subunit B and bound PL and sulfate molecules in the active site of subunit A. In the D235N mutant, after a similar refinement cycle, using a model with residue 235 as Gly, we observed a density extending from the α-carbon of residue 235 suggesting an Asn mutation. We also observed bound ATP and sulfate molecules in the active sites. The two complexes were refined with alternate cycles of conjugate gradient minimization, simulated annealing and B-factor refinements with intermittent model rebuilding using both TOM and COOT.[111, 112]

Addition of water, MPD and sulfate molecules led to the final crystallographic R_{work}/R_{free} of 21.2%/26.2% for the 2.5 Å resolution D235A structure; and 21.4%/26.1% for the 2.3 Å resolution D235N structure. The structure solution/refinement statistics are shown in Table 3. Atomic coordinates and structure factors have been deposited in the

RCSB Protein Data Bank with codes 3FHX and 3FHY for D235A and D235N, respectively.[16]

Table 3: Crystal information, data collection and refinement parameters of D235A and D235N mutants

	D235A	D235N
Data collection statistics		
Space Group	I222	I222
Cell Dimensions (Å)	91.2 115.4 168.9	91.1 114.6 169.7
Resolution (Å)[a]	32.69-2.5 (2.59-2.5)	32.54-2.30 (2.38-2.30)
No. of measurements	124056	133496
Unique reflections	31128 (2935)	39415(3745)
I/sigma I	10.9 (4.2)	15.5 (4.6)
Completeness (%)	99.7 (99.6)	99.0 (99.3)
Redundancy	3.99 (3.79)	3.39 (3.18)
R_{merge} (%)[b]	8.3 (29.8)	4.9 (25.0)
Structure refinement		
Resolution limit (Å)	29.93-2.5 (2.59-2.5)	29.36-2.30 (2.38-2.30)
No. of reflections	31124 (2935)	39410 (3745)
R_{work} (%)[c]	21.2 (38.9)	21.4 (38.2)
R_{free} (%)[d]	26.2 (40.3)	26.1(43.8)
Rmsd standard Geometry		
Bond-lengths (Å)	0.008	0.008
Bond-angles (°)	1.4	1.4
Dihedral angles		
Most favored regions	93.45	93.85
Additional allowed regions	5.73	5.32
Bfactors		
All atoms	43.8	44.22
Protein alone	43.2	43.40
ATP	40.7	38.45
Metal ions	35.3	28.42
Sulfate	72.3	74.07
Water	40.1	45.82
MPD	75.7	72.23

[a]Numbers in parentheses refer to the outer (highest) resolution shell.

[b] $R_{merge} = \sum|I - \langle I \rangle| / \sum(I)$, where I is the observed intensity and $\langle I \rangle$ is the weighted mean of the reflection intensity.

[c] $R_{work} = \sum||F_o| - F_c|| / \sum|F_o|$, where F_o and F_c are the observed and calculated structure factor amplitudes, respectively.

[d] R_{free} is the crystallographic R_{work} calculated with 5 % of the data that were excluded from the structure refinement.

3.3 Results and Discussion:

Three mutants D235H, D235A and D235N were constructed but only the latter two could be expressed and subsequently purified. The D235A mutant showed a 15-fold decrease in catalytic activity, as well as a 7-fold decrease in affinity for PL (Table 4). The D235N mutation resulted in a ~2-fold decrease in activity and PL affinity (Table 4). The K_m for MgATP did not change significantly between the wild-type and mutant enzymes (~200 uM), consistent with the fact that the carboxylate of Asp235 makes a hydrogen-bond interaction with PL but not with ATP.[12]

Table 4: Kinetic parameters for hPL kinase wild type and D235A and D235N mutants

Enzyme	Wild Type	D235N	D235A
K_m, Pyridoxal	24 μM	58 μM	170 μM
k_{cat}	29.37 Min^{-1}	14.39 Min^{-1}	1.9 Min^{-1}

X-ray structures of D235A and D235N mutants were determined to 2.5 and 2.3 Å, respectively. The D235A mutant structure, co-crystallized with PL and ATP, showed these two substrates, as well as the product PLP bound simultaneously at the subunit B active site (Figure 18A and B). In subunit A, we also observed PL and ATP, but instead of PLP, we found a bound sulfate molecule that occupies the PLP phosphate position.

The D235N mutant, co-crystallized with ATP, shows bound ATP and the sulfate molecule described above (Figure 18C and D). The sulfate molecules could be coming from $MgSO_4$ used in the crystallization experiment. However, we cannot rule out the possibility that this anion is phosphate results from spontaneous hydrolysis of ATP γ-phosphate, which is known to happen in PL kinase.[12] The PLP phosphate moiety or the sulfate molecule lies adjacent to the ATP γ-phosphate, and are stabilized by a P-loop, consisting of an anion hole formed by the highly conserved sequence motif GTGA (residues 231–234) and the N-terminus of the helix formed by the residues 234–248. The PLP phosphate or the sulfate molecule makes extensive hydrogen-bond interactions with the backbone nitrogen atoms of the anion hole residues, while the rest of the PLP molecule is located inside the active site with very limited protein contacts, consistent with a weaker PLP ring density. The ATP γ-phosphate is further stabilized by a bound Na^+, while the β-phosphate is stabilized by the P-loop and Mg^{2+}.

Comparisons of the D235A, D235N and the wild-type structures show similar folds with root mean square deviations of ~0.2 Å. The ATP and PL binding site geometries, as well as their associated interactions with the protein are also conserved (Figure 18 E). In the D235N mutant, the side-chain of Asn235 occupies the same position as the wild-type Asp235 side chain and makes a conserved hydrogen-bond interaction with the C5′-OH group of a modeled PL.

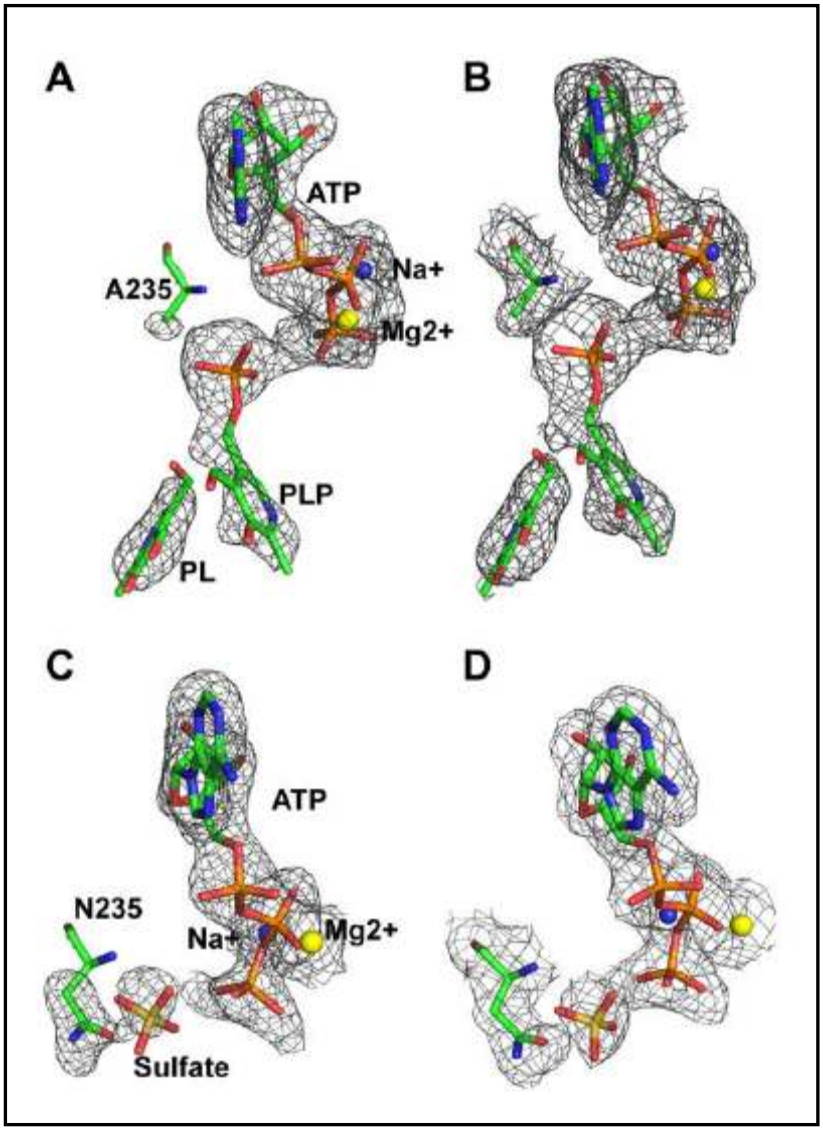

Figure 18: Crystal Structure of PL kinase mutants. (A) A Fo–Fc map (contoured at 2.6σ level) of the D235A model calculated before Na^{+}, Mg^{2+}, PLP, PL, ATP and Ala235 side-chain were added to the subunit B active site. (B) A 2Fo–Fc map (0.8σ level) of the subunit B active site of the D235A model. (C) A Fo–Fc map (2.6σ level) of the D235N model calculated before Na^{+}, Mg^{2+}, sulfate, and Asn235 side-chain were added to the subunit B active site. (D) A 2Fo–Fc map (0.8σ level) of the subunit B active site of the D235N model. All maps are superimposed with the final refined models.

In the D235A mutant, there is a non-conserved water molecule close to the Asp235 carboxylate oxygen atom (Figure 18 E). The water is close to the amide nitrogen of Gly20 (~3 Å), as well as the C5′-OH group of PL (~3 Å). The bound PL makes conserved PL kinase interactions with the residues Ser12, Thr47, Val19 and Tyr84.

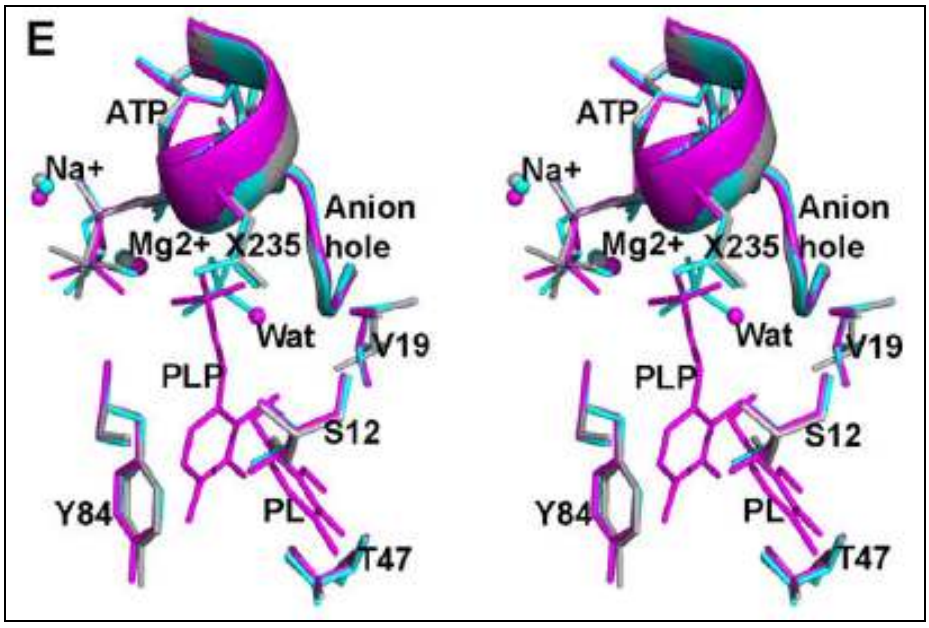

Figure 18: Crystal Structure of PL kinase mutants. (E) Stereo view comparison of the active site of the wild-type structure in complex with ATP (grey), D235N in complex with ATP and sulfate (cyan), and D235A in complex with PLP, PL, ATP and the non-conserved water (magenta). Residue 235 is labeled as X235. Also shown are the cation positions.

The study unexpectedly showed less than the anticipated drop in D235A mutant catalytic activity consistent with removal of an essential catalytic base. Since the human PL kinase enzyme was purified with a His-tag affinity column, significant contamination by wild-type enzyme is ruled out. Most likely, the observed activity of the D235A mutant could be attributed to the non-conserved water molecule described above acting as a weak

base. As reported before the ATP γ-phosphate is known to hydrolyze spontaneously,[12] which suggests that even a weak catalytic base could initiate the phosphorylation reaction.

Also, unexpectedly, we observe significant activity of the D235N mutant. It is not clear why this mutant is active, and we speculate that there could be another water molecule in the active site of this mutant which is acting as a base. However, the crystal structure did not identify such a water molecule, and it's possible this water molecule appears when the enzyme is in its pre-catalytic stage, which is not captured by the current structure.

This study suggests that Asp235 could be the catalytic base involved in PL kinase activity as depicted in Figure 17. In this mechanism, Asp235 forms strong hydrogen -bond with the 5′-OH of PL to enhance the nucleophilicity of the substrate. A subsequent nucleophilic attack by PL on the ATP γ-phosphate results in the transfer of the proton from the 5′-OH group to the Asp235 carboxyl group, and concomitant transfer of the γ-phosphate to PL. However, we cannot discount the fact that a water molecule at the active site could also be acting as a base. Most likely, the former may only be unique in the D235N mutant, where during the pre-catalytic state, the side chain of residue Asp235 makes a hydrogen-bond interaction with the "catalytic water" to increase its basic properties which subsequently makes nucleophilic attack on 5′-OH group of PL and deprotonates the substrate. Resultant, negatively charged O5′ atom of PL then makes a direct nucleophillic attack on the ATP γ-phosphate and complete the phosphorylation reaction with transfer of the γ-phosphate of ATP to PL (Figure 19).

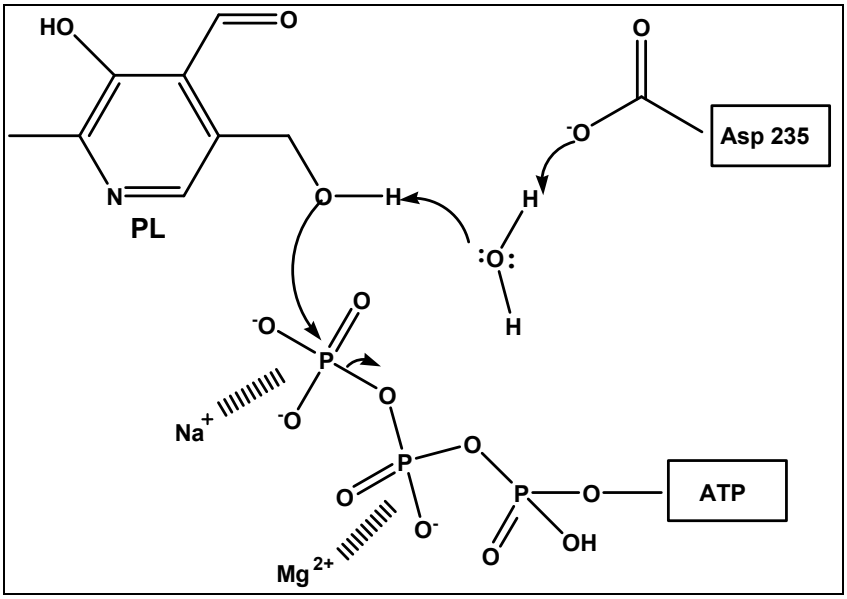

Figure 19: Alternate water mediated catalytic mechanism of PL kinase.

The reduced rate of PL phosphorylation by the D235A mutant might have led to the trapping of ATP, PL and PLP at the active site. The ability to trap a PLP in the presence of the MgATP substrate suggests that PL kinase might use this mechanism to self-regulate its activity. This is consistent with our kinetic study with *E. coli* PL kinase that showed severe MgATP inhibition of the enzyme in the presence of PLP.[8] We speculate that this inhibition is due to formation of a non-productive PL kinase·PLP·ATP complex.

3.4 Conclusion

Our kinetic studies document the catalytic role of Asp235 in PL kinase activity and suggest that Asp235 could act as the active site base to deprotonate pyridoxal prior to phosphorylation. The crystal structure of D235A shows bound ATP, PL and PLP, while D235N shows bound ATP and sulfate.[103] Other studies such as isotope studies are needed to reach definite conclusion about whether Asp235 is indeed acting as direct base for the phosphorylation reaction. The observation that the active site of PL kinase can accommodate both ATP and PLP suggests that formation of a ternary Enz•PLP•ATP complex could occur in the wild-type enzyme, consistent with severe MgATP substrate inhibition of PL kinase in the presence of PLP.

CHAPTER 4

Determine the Method of Kinetic Regulation of PL Kinase

4.1 Introduction: The crystal structures of PL kinase from several species, including *E. coli*, human and sheep PL kinases have been reported. The protein is a homodimer with an active site on each monomer composed of residues exclusively from each respective subunit. The active site starts as a shallow groove where ATP binds, and then stretches deeper into the protein where PL or PM or PN binds opposite but facing the γ-phosphate of the ATP. The residues that make interactions with both substrates are highly conserved among the PL kinase enzymes. The three ATP phosphate groups are stabilized by an anion hole formed by the highly conserved sequence motif GTGA and the N-terminus of a nearby helix, as well as by bound Mg^{2+} and K^{+} or Na^{+} respectively.[7-8, 11-12]

In most published PL kinase structures, the PL binding site is located about 6-7Å from the ATP, prompting the suggestion that the protein must undergo conformational change to a transition state that places the phosphate and the substrate closer together to allow for transfer of the γ-phosphate from ATP to the substrate.[7, 11-12] Consistently, a

ternary sheep PL kinase-ADP-PLP complex structure shows such a conformational change, and it's believed to represent the catalytic conformer.[11]

Disruption of the B_6 salvage pathway due to pathogenic mutations in PNP oxidase or PL kinase or inhibition of these two enzymes or lack of nutritional intake of vitamin B_6 is known to result in PLP deficiency, which has been implicated in several pathologies. On the other hand, intake of too much vitamin B_6 is known to result in toxic effects, including sensory and motor neuropathies. This is due in part to the PLP aldehyde propensity to react with several nucleophiles including non-B6 enzyme in the cell.[46, 48-50] Maintaining a low level of PLP *in vivo* (~1 uM) through hydrolysis of free PLP to PL by phosphatases is one of the ways the cell has solved this problem. Consistently, the k_{cat} values of phosphatases are 30-fold higher than that of PL kinase.[6] A second suggested mechanism, but not well documented, is through PL kinase and/or PNP oxidase regulation. A recent study with ePL kinase showed severe induced MgATP substrate inhibition of the enzyme in the presence of its product, PNP or PLP. It was suggested that some control mechanism is operating for PL kinase reaction.[8] Kinetic and structural studies of hPL kinase with its substrates and products were performed to gain insight into the regulation of PLP by PL kinase.

4.2 Methods

4.2.1 MgATP substrate inhibition studies: Human PL kinase was expressed and purified as described earlier in chapter 3, section 3.2.1. The enzyme was dialyzed overnight against 20 mM sodium BES buffer, pH 7.2. Kinetic assays were performed at 37 °C in a 1 cm thermostated cuvette. Initial velocity studies for the conversion of PL to

PLP were followed at 388 nm in an Agilant 8454 spectrophotometer in 20 mM sodium BES buffer, pH 7.2.[9, 92] MgATP substrate inhibition studies of hPL kinase (285 μM) were carried out at a fixed concentration of substrate PL (150 μM) and variable concentration of ATP from 60 to 300 μM and three different fixed PLP concentrations of 100, 150 and 250 μM.

4.2.2 ADP product inhibition studies: Kinetic constants and mode of inhibition for ADP were also determined at three different ADP concentration of 200, 400 and 800 μM at a saturating PL concentration of 1 mM and varied MgATP concentrations between 200 μM and 1200 μM.

4.2.3 Crystallization, data Collection and structure determination: A complex mixture of hPL kinase (36 mg/ml enzyme in 20 mM Sodium BES buffer, pH 7.2, containing 150 mM NaCl and 5 mM BME) and 2.5 mM each of MgATP and PLP were incubated on ice for about 3–4 h. The complex was crystallized using precipitant composed of 100 mM Tris-HCl, pH 8.0, 52% MPD and 2.5 mM $MgSO_4$. For data collection, crystals were first cryoprotected in solution containing 100 mM Tris-HCl buffer (pH 8.0) and 50% MPD with 2.5 mM PLP and MgATP. X-ray data were collected at 100 K using a Molecular Structure Corporation (MSC) X-Stream Cryogenic Crystal Cooler System and an R-Axis IV++ image plate detector, a Rigaku MicroMax–007 X-ray source equipped with MSC Varimax confocal optics operating at 40 kV and 20 mA.

The isomorphous hPL kinase structure (PDB code 2YXT)[9], omitting bound phosphate, water and MPD molecules was used as the starting model for the refinement using the CNS program.[96] After rigid body refinement, and subsequent conjugate gradient

minimization and simulated annealing, difference density consistent with ATP, Mg^{+2} and Na^{+} were observed at both active site. In addition, difference density consistent with a mixture of bound PLP and MPD was also identified at the PL binding site at both active site. These molecules and ligands were added to the models, and the structure subsequently refined with alternate cycles of conjugate gradient minimization, simulated annealing and B-factor refinements with intermittent model rebuilding with TOM and COOT.[111, 112]

Addition of water, MPD and sulfate molecules led to the final crystallographic R_{work}/R_{free} of 20.9%/25.6%. COOT was used for structure validation. Structure solution/refinement statistics are shown in Table 5. Atomic coordinates and structure factors for the structure of hPL kinase in complex with ATP and PLP have been deposited in the RCSB Protein Data Bank with accession code 3KEU.

Table 5: Refinement parameters for the human PL kinase structure with bound ATP and PLP

Data collection statistics	
Space Group	I222
Cell Dimensions (Å)	91.20, 114.58, 169.41
Resolution (Å)[a]	26.98 – 2.00 (2.07-2.00)
No. of measurements	184435
Unique reflections	59477 (5949)
I/sigma I	13.3 (3.4)
Completeness (%)	98.9 (99.0)
R_{merge} (%)[b]	4.9 (30.0)
Structure refinement	
Resolution limit (Å)	26.98 – 2.10 (2.18-2.10)
No. of reflections	51485 (4801)
R_{work} (%)[c]	20.9 (40.3)
R_{free} (%)[d]	25.6 (44.5)
Rmsd standard Geometry	
Bond-lengths (Å)	0.010
Bond-angles (°)	1.60
Dihedral angles	
Most favored regions	91.1
Additional allowed regions	8.9
Bfactors	
All atoms	43.52
Protein alone	42.40
ATP	37.20
PLP	69.30
Metal ions	43.11
Sulfate	62.56
Water	51.55
MPD	66.31

[a]Numbers in parentheses refer to the outer (highest) resolution shell.

[b] $R_{merge} = \sum|I - \langle I \rangle| / \sum(I)$, where I is the observed intensity and $\langle I \rangle$ is the weighted mean of the reflection intensity.

[c] $R_{work} = \sum||F_o| - F_c|| / \sum|F_o|$, where F_o and F_c are the observed and calculated structure factor amplitudes, respectively.

[d] R_{free} is the crystallographic R_{work} calculated with 5 % of the data that were excluded from the structure refinement.

4.3 Results and discussion

4.3.1 Severe MgATP substrate inhibition of PL kinase in the presence of PLP and evidence of tight PLP binding in PL Kinase: In our previously published study with ePL kinase, we observed severe substrate inhibition by MgATP in the presence of PLP or PNP, suggesting some possible control mechanism is operating for products of the kinase reaction.[8] At 200 μM ATP there is a 60% inhibition of activity. The cellular concentration of ATP is estimated to be near 400 μM in cells, suggesting that this level of ATP would result in almost total inhibition of the kinase activity in the presence of 250 uM PLP. We have repeated this experiment with hPL kinase using PLP (100-250 μM). Figure 20 shows inhibition pattern of hPL kinase with PLP as a product inhibitor at a fixed concentration of substrate PL and variable concentration of MgATP.

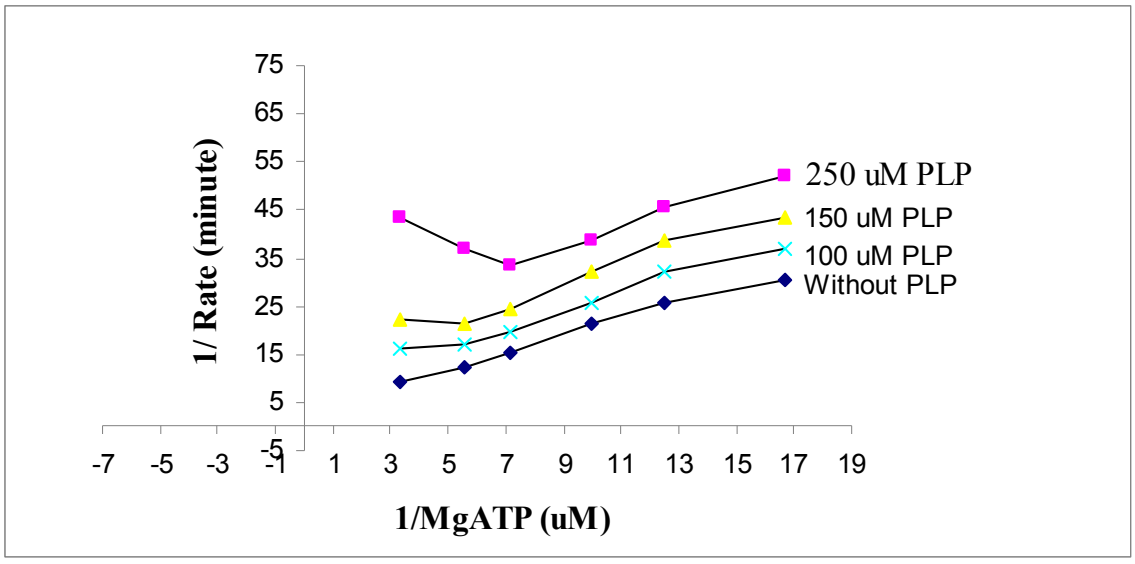

Figure 20: MgATP substrate inhibition of human PL kinase in the presence of PLP

As previously observed in the study with ePL kinase, the sharp upward curvature in the above double reciprocal plot in the presence of PLP is most likely the result of MgATP substrate inhibition, and at 150 μM of ATP, we observe 50% inhibition.[8] This inhibition mechanism could be a physiological regulatory process utilized by PL kinase to keep the level of PLP low in the cell as a free molecule. Intracellular concentrations of enzymatic reactions products are maintained at certain level and one way the cell regulates the activity of enzymes is feedback inhibition that shut down the biochemical pathway to avoid excess product concentration. Native gradient gel analysis rules out protein oligomerization as a possible reason for the observed inhibition.

Interestingly, the PLP in the PL kinase/MgATP complex was found to be tightly bound as dialyzing the ternary complex overnight in the presence of MgATP, and then running it down a 15 cm column of BioGel P6-DG equilibrated with a buffer containing Na-BES and MgATP did not remove the bound PLP. Also of note is that the tightly bound PLP in the PL kinase/MgATP complex is released in the presence of a PLP-dependent enzyme, apo-SHMT (serine hydroxymethyltransferase) to activate the enzyme into its holo-form. We hypothesize the source of this inhibition to be due to formation of a non-productive ternary PL kinase complex of ATP and PLP (PL kinase•PLP•ATP), and that both PLP and ATP bind at the active site. Analysis of previous ligand complex structures of PL kinase suggests that this ternary complex could form since the 5'-OH of PL is located 6-7 Å from the γ-phosphate of ATP, the space sufficient enough to allow coexistence of the C5' phosphate ester of PLP with the γ-phosphate of ATP (Figure 21). In support of this supposition is the fact that our recently published PL kinase D235A mutant

structure shows ATP and PLP trapped at the active site.[16] If this hypothesis is proven correct, it will be a unique case because in most feedback inhibition, the enzymatic product confers its inhibitory activity by binding to a non-catalytic or allosteric site. For example, L-threonine deaminase is involved in catalytic conversion of L-threonine to L-isoleucine, and the enzyme is strongly inhibited by L-isoleucine at an allosteric site.[113] Also, aspartate kinase which catalyzes the phosphorylation of the amino acid aspartate which is a first step in the biosynthesis of methionine into threonine and lysine, is also inhibited by its product at an allosteric site.[114]

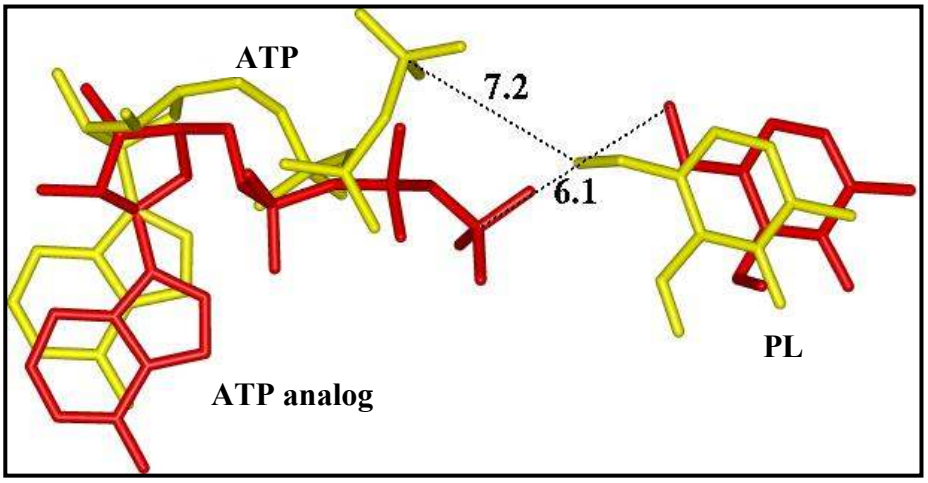

Figure 21: Superposition of the ATP and PL bound complex of ePL kinase (colored yellow) and the ternary ATP analog/PM crystal structure of sheep kinase (colored red). PL-bound ePL kinase crystal structure and MgATP-bound ePL kinase crystal structure were superimposed on each other to obtain ATP and PL bound complex of ePL kinase.

4.3.2 ADP product inhibition of PL kinase: Above, we show that the substrate MgATP of the kinase can inhibit the enzyme in the presence of its product, PLP. To find out whether the enzymatic product, ADP could also inhibit the PL kinase activity, we performed experiments to determine the *Ki* of ADP at fixed saturating concentration of PL and varied concentration of ATP. Note that ADP binds at the same place as the substrate ATP. Kinetic studies were carried out at three different ADP concentration of 200, 400 and 800 μM at a saturating PL concentration of 1 mM and varied MgATP concentrations between 200 μM and 1200 μM. Data showed ADP competitively inhibited ATP with *Ki* of 361 μM (Figure 22).

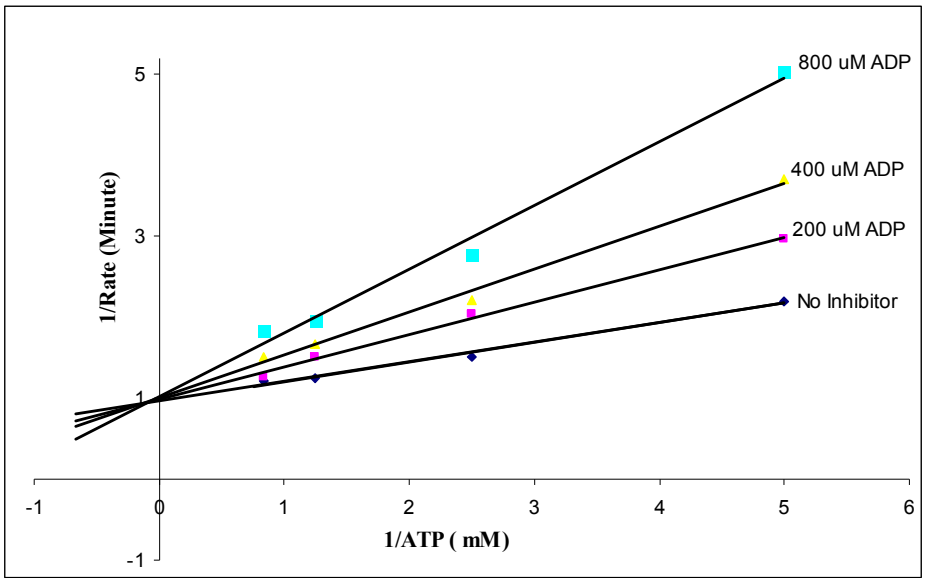

Figure 22: Determination of binding constants for ADP

4.3.3 MgATP and PLP bind to PL kinase to form a ternary complex: To test our hypothesis that the observed hPL kinase inhibition by MgATP in the presence of PLP

is due to the formation of a non-productive ternary complex of PL kinase•PLP•MgATP, we co-crystallized hPL kinase with PLP and MgATP. The structure was refined to 2.1 Å, using an already published isomorphous hPL kinase structure (PDB code 2YXT).[9] The root mean square deviation between the two protein dimers is ~0.25Å, indicating similar overall conformation. The complex structure showed both ATP and PLP bound in both subunit active sites (Figure 23, 24). The PLP occupies the PL binding site. We also observe a bound MPD in later refinement cycles overlapping the bound PLP pyridine ring. The PLP and MPD were refined using 50% occupancy for each molecule.

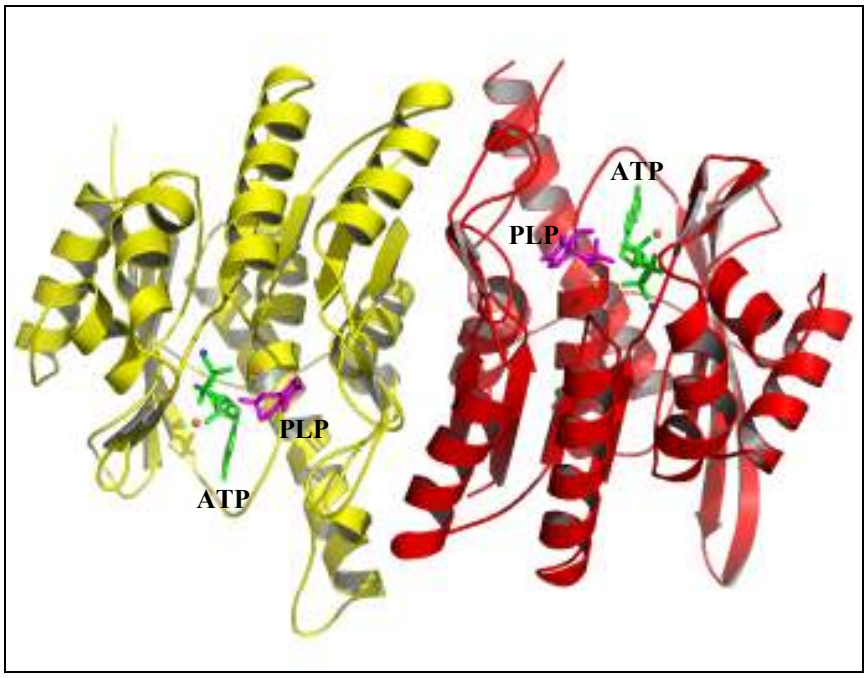

Figure 23: The dimeric structure, of human PL kinase with bound ATP (green), PLP (magenta), Na^{+} (blue sphere), and Mg^{2+} (orange sphere). MPD molecule at both the active site is not shown for clarity. Monomers A and B are colored red and yellow, respectively.

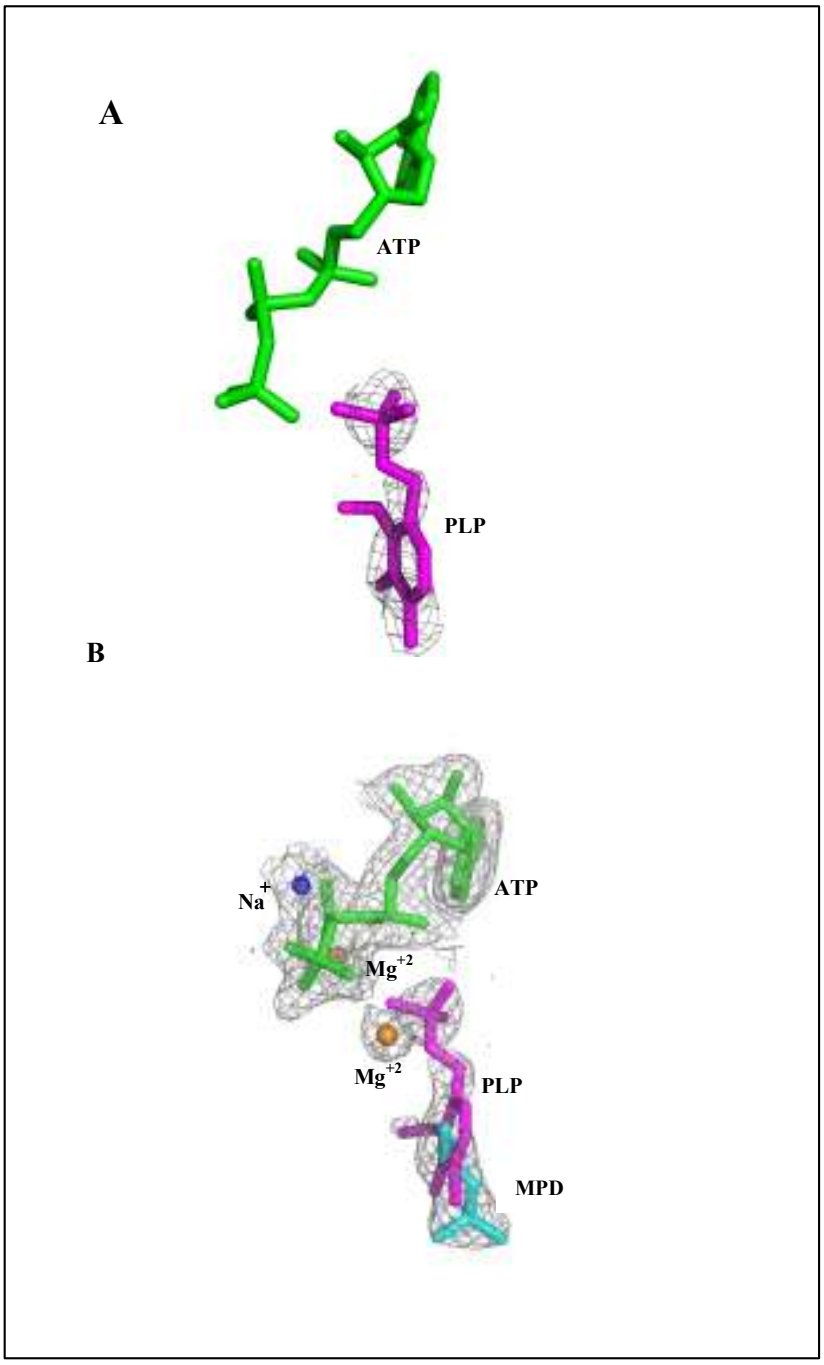

Figure 24: Crystal Structure of human PL kinase with ATP and PLP and MPD (A) A Fo–Fc map (contoured at 2.6σ level) calculated before PLP was added to the subunit B active site. (B) A 2Fo–Fc map (0.8σ level) of the subunit B active site. All maps are superimposed with the final refined models.

As previously observed, binding of ATP in the ternary complex is stabilized by a P-loop consisting of an anion hole formed by the highly conserved sequence motif GTGA (residues 231-234) and the N-terminus of the helix formed by the residues 234-248.[9,103] The ATP binding is also stabilized Mg^{+2} and Na^{+} close to the phosphates of the ATP. Other interactions between the ATP and the protein are all conserved. [9,103] The PLP binds at the PL site, where the pyridine moiety makes conserved interactions with the residues Ser12, Thr47 and Tyr84. However, these interactions are weaker compared to PL interactions due to the fact that the pyridine moiety of PLP is displaced about ~2 Å from the PL ring position. Interestingly, overlapping the pyridine moiety was an MPD molecule.

The PLP phosphate ester extends toward the ATP phosphate to lie adjacent to the ATP γ-phosphate. Most significantly, we observe a second Mg^{+2} making interactions to both the PLP phosphate and the ATP γ-phosphate moieties, as well as to Asp235 that should stabilize the two phosphate positions. In addition, extensive hydrogen-bond interactions from the P-loop to the phosphates of ATP and PLP are also essential for stabilization of the two ligands (Figure 25).

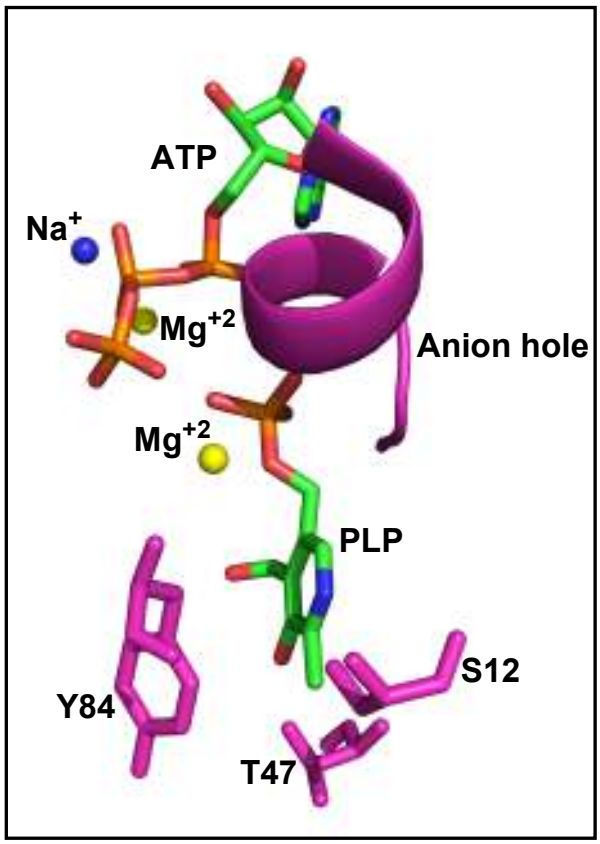

Figure 25: Crystal Structure of Human PL kinase in complex with bound ATP and PLP: Active site of the wild-type structure in complex with PLP, ATP. Also shown are the cation positions.

4.4. Conclusion

Accumulation of the PLP in the cell as a free molecule must be kept low since it can rapidly react with amines, proteins, and thiols to form adducts.[44-50] The cell has evolved mechanisms for regulating PLP synthesis and we hypothesize that one of these mechanisms involve PL kinase. Our studies suggest that PL kinase could be using its substrate and/or enzymatic product to self-regulate its activity.[16] Kinetic and structural studies strongly point to a formation of non-productive ternary complex

(Enzyme•PLP•MgATP) as the basis of the kinase activity inhibition. Further studies are needed to conclusively prove such an inhibitory mechanism. Our studies also show that ADP is a competitive inhibitor of the enzyme with a K_i of 361 μM.

CHAPTER 5

Identify Drugs and Other Compounds that are Inhibitors of PL Kinase

5.1 Introduction: Some drugs inhibit the activity of PL kinase, which result in disruption of B_6 metabolism and PLP deficiency with concomitant neurotoxic adverse effects such as sleeplessness, headache, restlessness, agitation, tremors and hallucinations. Examples of these drugs are isoniazid, theophylline**,** progabide, cycloserine, L-DOPA, penicillamine, and steroid contraceptives.[53-61] We hypothesize that other drugs and natural products that cause similar side effects as theophylline and other PL kinase inhibitors could also be depleting PLP in the cell by inhibiting PL kinase activity. Kinetic and structural studies of hPL kinase in the presence of several potential PL kinase inhibitors were performed.

5.2 Methods

5.2.1 Selection of compounds for inhibition study: Theophylline is a bronchodilator and its use has been associated with neurotoxic side effect due to its inhibitory effect against PL kinase that leads to vitamin B_6 deficiency. Interestingly, enprofylline, theobromine and caffeine (Figure 26), structural analogs of theophylline also

exhibit similar neurotoxic effects as theophylline. Although, there is no evidence or prior studies to suggest that PL kinase inhibition is the cause of their neurotoxic side effects, we decided to study their inhibitory activity against the enzyme due to their structural similarities with theophylline.[54-58] We also decided to study the inhibitory activities of other drugs on PL kinase, including epinephrine, lamotrigine, metaraminol, and mesalamine (Figure 23). These drugs also exhibit similar neurotoxic effects as theophylline, and most importantly they have similar structural characteristics as the natural substrate, PL or the theophylline.[62, 55] They were identified from the DrugBank Chemical Compound database using PL or theophylline as search queries.

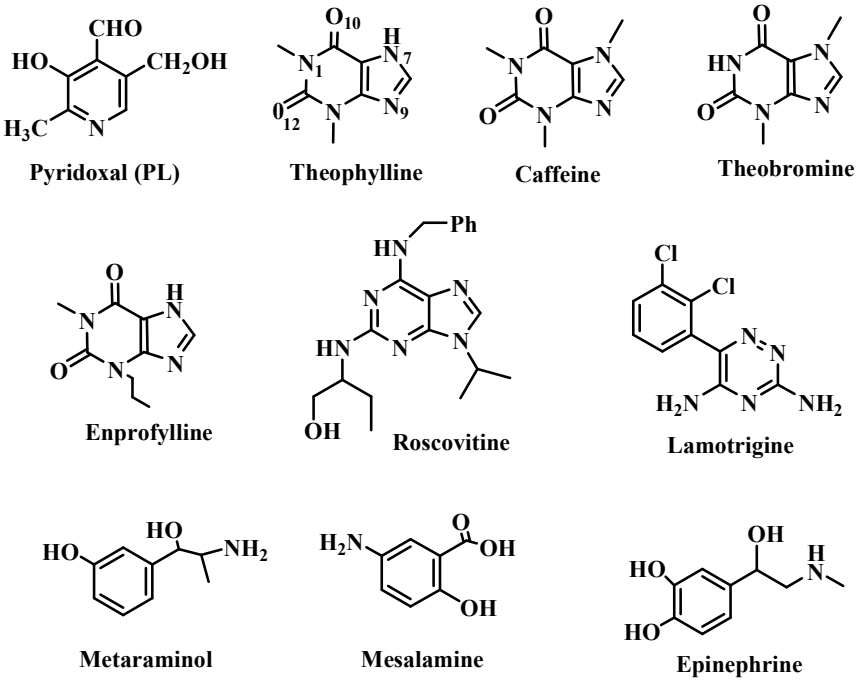

Figure 26 : Selected neurotoxic drugs for inhibition studies

5.2.2 Determination of inhibition constants: Human PL kinase was expressed and purified as described earlier in Chapter 3, section 3.2.1. Fractions containing 95% purity, as judged by SDS-Page, were pooled and the protein solution was concentrated by

precipitation with 60% ammonium sulfate. Human PL kinase used in the kinetic experiments was dissolved and dialyzed overnight against 20 mM sodium BES buffer, pH 7.2. All assays were performed at 37ºC in a 1-cm thermostated cuvette. Initial velocity studies for the conversion of PL to PLP were followed at 388nm in an Agilant 8454 spectrophotometer in 20 mM sodium BES buffer, pH 7.2.[9, 92] As a first step, percentage inhibition of hPL kinase with each tested drug (100 μM) was measured at a saturating MgATP concentration of 1 mM and fixed PL concentration of 75 uM. Detailed kinetic studies to determine K_i and mode of inhibition for the drugs showing more than 30% inhibition were carried out at three different drug concentrations of 50, 100 and 150 μM under two experimental conditions: at a saturating MgATP concentrations of 1 mM and varied PL concentrations between 20 and 100 μM, and reciprocally at a saturating PL concentrations of 500 μM and varied MgATP concentrations between 150 and 800 μM. Inhibition constants were determined by double reciprocal plots.

5.2.3 Crystallization, data Collection, and structure refinement: Human PL kinase protein was dialyzed overnight against 20 mM Sodium BES buffer, pH 7.2, containing 150 mM NaCl and 5 mM BME, and then concentrated to 36mg/ml (1 mM). Crystallization of hPL kinase in the presence of 2.5 mM theophylline/ or caffeine/ or enprofylline/ or lamotrigine was attempted at room temperature using the hanging-drop vapor diffusion technique. The complex mixtures were first incubated on ice for about 1-2 hr before screening for crystallization.

Crystallization drops were composed of 2.5 μL of protein solution (with 2.5 mM drug) and 2.5 μL of reservoir and equilibrated against 700 μL reservoir solution (100 mM

Tris-HCl, pH 8.0, and 52% MPD, 2.5 mM $MgSO_4$). X-ray quality crystals were obtained for only the protein-theophylline complex. For data collection, crystals were cryoprotected in solution containing 100 mM Tris-HCl buffer (pH 8.0), 2.5 mM theophylline and 50% MPD before flash cooling in a cryogenic nitrogen gas stream. X-ray data were collected at 100 K using a Molecular Structure Corporation (MSC) X-Stream Cryogenic Crystal Cooler System and an R-Axis IV++ image plate detector, a Rigaku MicroMax–007 X-ray source equipped with MSC Varimax confocal optics operating at 40 kV and 20 mA.

The isomorphous hPL kinase wild type structure (PDB code 2YXT), [9] and omitting bound phosphate, water and MPD molecules was used as the starting model for the refinements of the theophylline bound structure. All refinements were performed with the CNS program.[96] A statistically random selection of 5 % of the total reflection data was excluded from the refinement and used to calculate the R_{free} as a monitor of model bias. After rigid body refinement, and subsequent conjugate gradient minimization, simulated annealing and B-factor refinements, theophylline density was identified at the PL binding site in the A subunit. However, the B subunit active site was found to be occupied by an MPD molecule. Densities were also identified for Na^+ in both subunit active sites.

These molecules and ligands were added to the model, and the ensuing model subsequently refined with alternate cycles of conjugate gradient minimization, simulated annealing and B-factor refinements with intermittent model rebuilding with TOM and COOT.[111, 112] Addition of 337 water, 12 MPD and 7 sulfate molecules led to the final crystallographic R_{work}/R_{free} of 20.2%/25.5%. COOT was used for structure validation. The structure solution/refinement statistics are shown in Table 6. Atomic coordinates and

structure factors for the structure of hPL kinase in complex with theophylline have been deposited in the RCSB Protein Data Bank with accession code 3KBI.

Table 6: Refinement parameters for the human PL kinase structure with bound theophylline

Data collection statistics	
Space Group	I222
Cell Dimensions (Å)	92.30, 115.85, 171.90
Resolution (Å)[a]	37.68 – 2.10 (2.18-2.10)
No. of measurements	157598
Unique reflections	52989 (5317)
I/sigma I	18.5 (4.1)
Completeness (%)	98.1 (98.0)
R_{merge} (%)[b]	3.2 (24.1)
Structure refinement	
Resolution limit (Å)	29.19 – 2.10 (2.18-2.10)
No. of reflections	52986 (4941)
R_{work} (%)	20.4 (33.5)
R_{free} (%)[c]	25.5 (37.2)
Rmsd standard Geometry	
Bond-lengths (Å)	0.007
Bond-angles (°)	1.30
Dihedral angles	
Most favored regions	91.6
Additional allowed regions	8.4
Bfactors	
All atoms	48.15
Protein alone	46.79
Theophylline	85.78
Metal ions	95.42
Sulfate	66.13
Water	55.94
MPD	75.83

[a]Numbers in parentheses refer to the outer (highest) resolution shell.

[b] $R_{merge} = \sum|I - \langle I \rangle| / \sum(I)$, where I is the observed intensity and $\langle I \rangle$ is the weighted mean of the reflection intensity.

[c] $R_{work} = \sum||F_o| - |F_c|| / \sum|F_o|$, where F_o and F_c are the observed and calculated structure factor amplitudes, respectively.

[d] R_{free} is the crystallographic R_{work} calculated with 5 % of the data that were excluded from

the structure refinement.

5.3 Results and Discussion

5.3.1 Inhibition studies: Initial inhibition studies revealed some of the tested drugs (Figure 26) as hPL kinase inhibitors, with theophylline being the most potent (Table 7). Subsequently, detailed kinetic studies of the drugs showing more than 30% inhibition were carried out to determine K_i and mode of inhibition. Double reciprocal plots of reaction velocities against PL or MgATP concentrations in the presence and absence of theophylline show a mixed competitive inhibition profile with K_i values of 71 μM and 225 μM, respectively (Figure 27). This result suggests theophylline could be binding to substrate PL site, and the mixed competitive behavior is likely due to the fact that binding of PL and ATP are synergistic. It is also quite possible that theophylline could be binding at both PL and ATP site, as we have previously observed for MPD molecules.[9] Previous studies with theophylline using non-purified PL kinase enzyme based on HPLC separation and fluorometric detection of PL and PLP also reached similar conclusions.[55]

Enprofylline, theobromine and caffeine are structural analogs of theophylline (Figure 26), and the first two compounds, like theophylline, are bronchodilators and had been used for treating asthma.[56] Enprofylline, caffeine and theobromine also showed inhibitory actions against hPL kinase, resulting in 33%, 22% and 21% inhibition at 100 μM, respectively. Detailed inhibition studies of human PL kinase with enprofylline revealed mixed competitive inhibition with K_i of 228 μM. Lamotrigine, also showed mixed competitive inhibition profile with K_i of 160 μM and this result correlates well with other studies that reported a drop in serum concentration of PLP of epileptic patients when treated with anticonvulsants, such as lamotrigine.[62] We did not observe any significant hPL kinase inhibition with the drugs, epinephrine, mesalamine, and metaraminol.

Table 7: Kinetic parameters of human PL Kinase inhibition by drugs

Compound	% Inhibition[a]	K_i (uM)[b]	Inhibition Mechanism [b]
Theophylline	60	71	Mixed
Theobromine	21	ND	ND
Caffiene	22	ND	ND
Enprofylline	33	228	Mixed
Epinephrine	Null	ND	ND
Metaraminol	Null	ND	ND
Mesalamine	Null	ND	ND
Lamotrigine	45	160	Mixed

[a] PL, ATP and drug concentrations of 75 uM, 1 mM and 100 uM, respectively.

[b]At variable PL and saturated ATP. [d]ND (not determined yet).

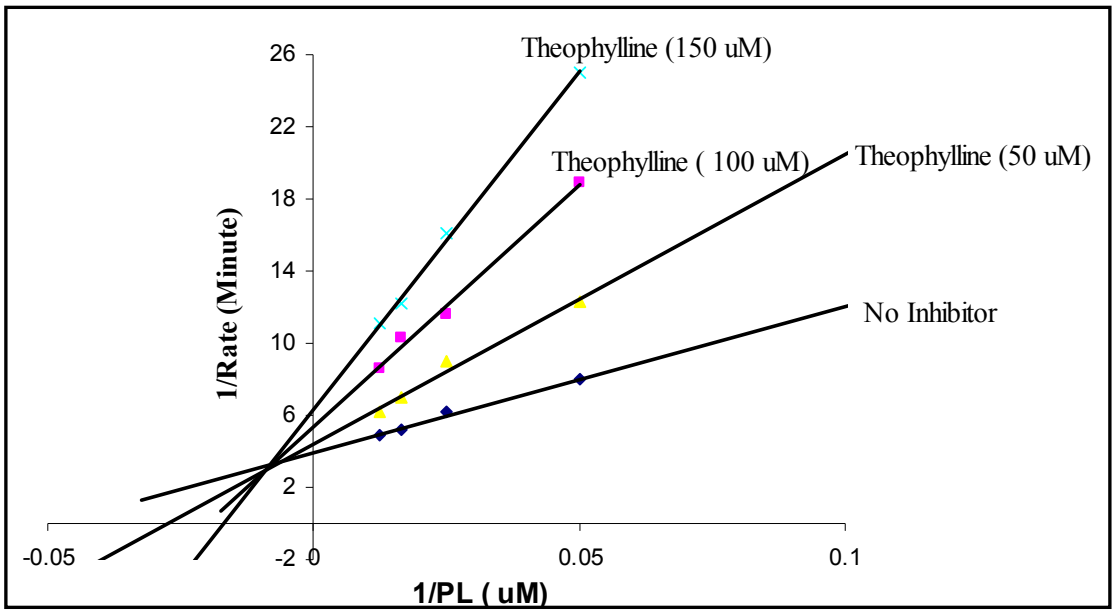

Figure 27: Determination of binding mode and inhibition constants of Theophylline

5.3.2 Structure of PL kinase-Inhibitor Complex Our inhibition studies suggest that theophylline and the other compounds could be binding to the active site of PL kinase, and inhibiting the enzyme. We therefore undertook structural studies to determine the precise binding modes of these compounds. Human PL kinase was co-crystallized with theophylline and refined to 2.1 Å, using the isomorphous hPL kinase structure (PDB code 2YXT).[9] Other compounds, including caffeine, enprofylline and lamotrigine were also co-crystallized with hPL kinase, but we were unable to obtain X-ray quality crystals. The crystal structure showed bound theophylline at the PL binding site (Figure 28, 29). Even

though we observe mixed inhibition, there was no obvious binding of theophylline at the ATP site, which could be due to weak binding.

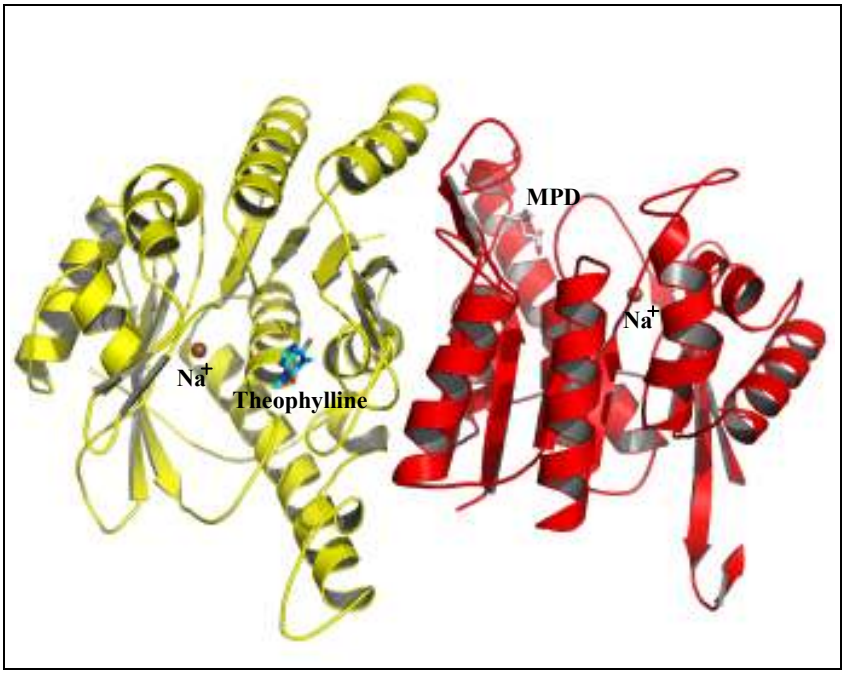

Figure 28: The dimeric structure, of human PL kinase with bound Thephylline, MPD, Na^+ (brown sphere). Monomers A and B are colored red and yellow, respectively.

A hydrogen-bond interaction is formed between N^7 of theophylline and the hydroxyl group of Ser12 side-chain. The N^7 and $N^9$of theophylline are also involved in hydrogen bond interactions with nearby water molecules. These water molecules make interactions with the main-chain nitrogen atom of residue Ser12, and the anion hole residue Gly231. The anion hole is formed by the highly conserved sequence motif GTGA (residues 231-234) that stabilizes bound ATP.[9] There are also hydrogen-bond interactions between O^{10} and O^{12} of theophylline with the hydroxyl group of Ser12 and Thr47, respectively. The O^{12} atom also makes hydrogen-bond interaction with main-chain nitrogen atom of Thr47. Theophylline also makes an apparent π- π interaction with Tyr84. Other hydrophobic interactions are made to Val19 and Val231. These hydrogen-bond and

hydrophobic interactions are also observed with PL binding. We observed theophylline density in only A subunit. Also, of note is that Roscovitine, a PL kinase inhibitor, is also known to bind at the same position as theophylline and makes similar protein interactions.[70-71] Roscovitine has strikingly similar core structural features as theophylline (Figure 29, 30).

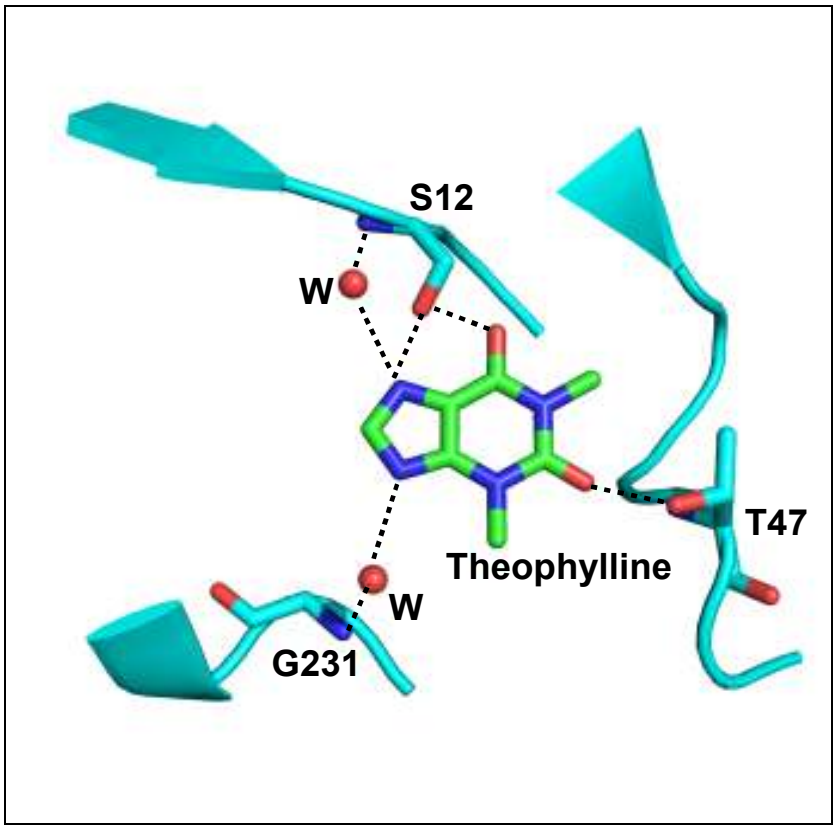

Figure 29: Interactions between theophylline, human PL kinase active site residues serine 12(S12), threonine 47 (T47), glycine 231 (G231), and water (W). Hydrogen-bond interactions are denoted with dotted lines.

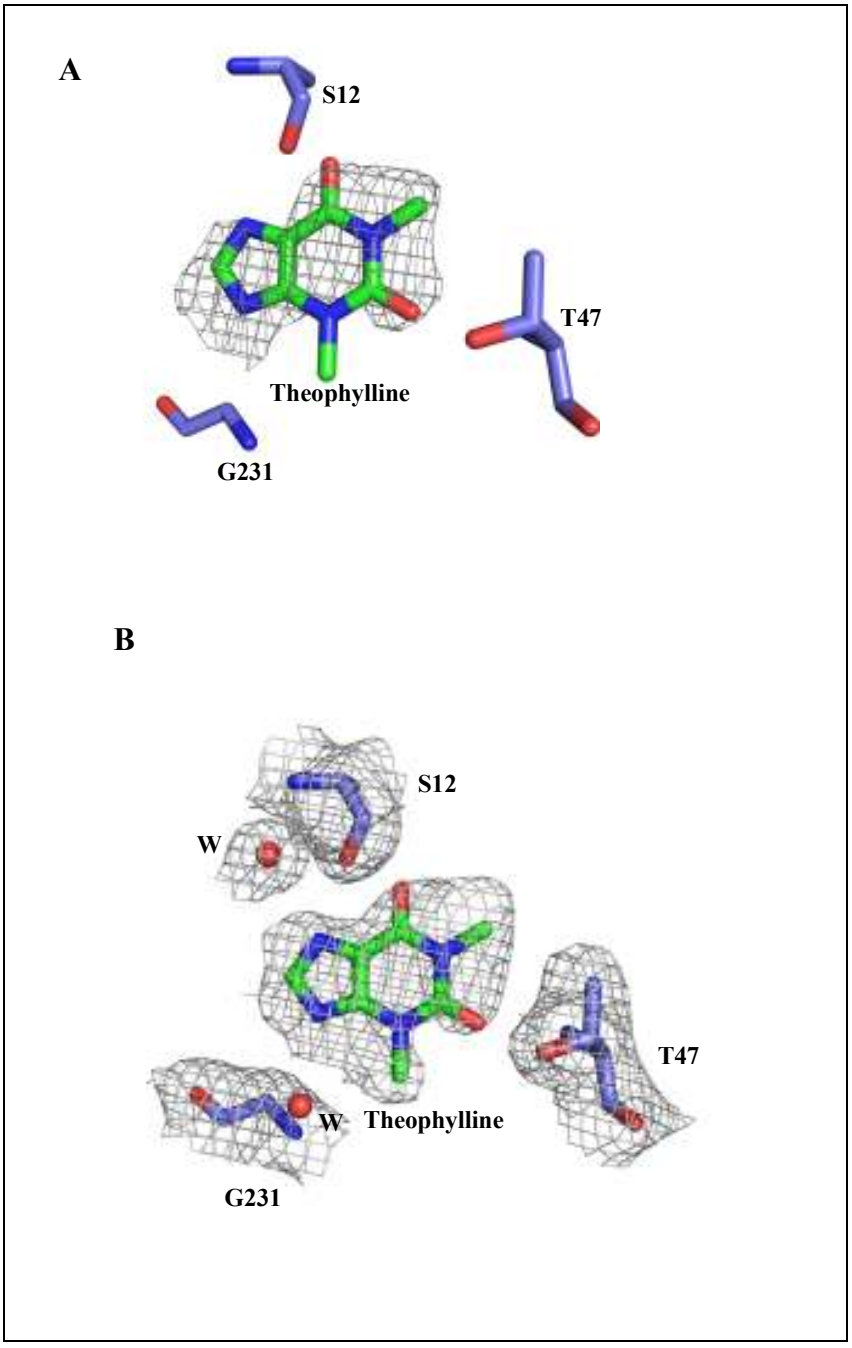

Figure 30 : Crystal Structure of human PL kinase with theophylline and active site residues serine 12(S12), threonine 47 (T47), glycine 231 (G231), and water (W). **A**: A Fo–Fc map (contoured at 2.7σ level) calculated before theophylline was added to the subunit A active site.
B: A 2Fo–Fc map (0.8σ level) of the subunit A active site. All maps are superimposed with the final refined models.

In the absence of crystal structures for the structural analogs of theophylline, we decided to visually model these compounds based on theophylline binding mode to gain insight into the structural basis of the differences in their inhibitory activities. The significantly lower affinity of caffeine and theobromine seems to be due to the imidazole nitrogen, N^7 being methylated and not available to make hydrogen-bond interactions with the nearby Ser12 hydroxyl group and water molecule as observed in theophylline. Although, not obvious it seems that the reduced affinity of enprofylline compared to theophylline could be due to steric crowding by the enprofylline propyl moiety (Figure 31).

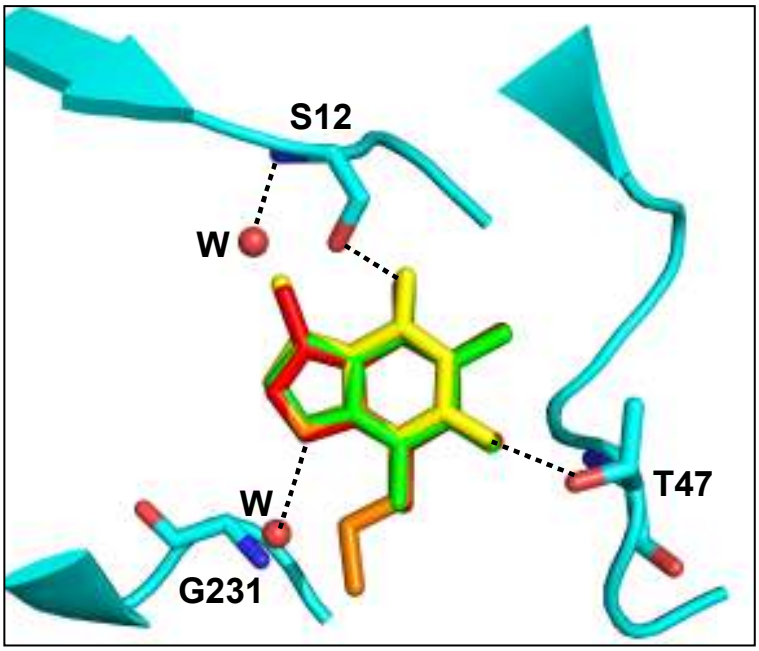

Figure 31: Binding modes of caffeine (red), theobromine (yellow), enprofylline (orange), and theophylline (green) at the active site of hPL kinase. Active site residues serine 12(S12), threonine 47 (T47), glycine 231 (G231), and Water (W) are shown. Hydrogen-bond interactions are denoted with dotted lines.

5.4 Conclusion

Many studies have reported several drugs, as well as natural compounds, that inhibit PL kinase activity resulting in PLP deficiency with concomitant neurotoxic effects.[53-61] We tested 8 drugs identified as potential PL kinase inhibitors based on their neurotoxic properties and similar structural features as PL or theophylline. Out of the 8 compounds, 5 showed significant inhibitory activities against PL kinase, while three did not. Lamotrigine, theophylline and its structural analogs, including enprofylline, theobromine and caffeine inhibited hPL kinase. Structural studies also confirm the results of the kinetic studies which suggest that theophylline bind at the PL binding site resulting in PL kinase inhibition. The result of this study suggests that neurotoxic effects of some drugs could be due to their inhibitory activity against PL kinase by disrupting the binding of the B6 substrate. More studies, including cell-based and possibly *in-vivo* with some of these inhibitors are planned to determine the effect of these compounds on vitamin B6 pool.

Literature Cited

1. Coburn S. P., Slominski A., Mahuren J. D., Wortsman J., Hessle L. and Millan J. L. Cutaneous metabolism of vitamin B6. *J. Invest. Dermatol,* **2003**, *120*, 292-300.
2. Belitsky B. R. Physical and enzymological interaction of Bacillus subtilis proteins required for de novo pyridoxal 5'-phosphate biosynthesis. *J. Bacteriol,* **2004**, *186***,** 1191- 1196.
3. Wetzel D. K., Ehrenshaft M., Denslow S. A. and Daub M. E. Functional complementation between the PDX1 vitamin B6 biosynthetic gene of Cercospora nicotianae and pdxJ of Escherichia coli. *FEBS Lett,* **2004,** *564,* 143-146.
4. McCormick D. B., and Chen H. Update on interconversions of vitamin B6 with its coenzyme. *J. Nutr***, 1999**, *129***,** 325-327.
5. Sivaraman J., Li Y., Banks J., Cane D. E., Matte A. and Cygler M. Crystal structure of Escherichia coli PdxA, an enzyme involved in the pyridoxal phosphate biosynthesis pathway. *J. Biol. Chem,* **2003**, *278***,** 43682-43690.

6. Li T. K., Lumeng L. and Veitch R. L. Regulation of pyridoxal 5'-phosphate metabolism in liver. *Biochem. Biophys. Res. Commun.,* **1974***, 61***,** 677-684.

7. Safo M. K., Musayev F. N., Hunt S., di Salvo M. L., Scarsdale N. and Schirch V. Crystal structure of the PdxY Protein from Escherichia coli. *J. Bacteriol,* **2004,** *186,* 8074-8082.

8. Safo M. K., Musayev F. N., di Salvo M. L., Hunt S., Claude J. B. and Schirch V. Crystal structure of pyridoxal kinase from the Escherichia coli pdxK gene: implications for the classification of pyridoxal kinases. *J. Bacteriol,* **2006,** *188,* 4542-4552.

9. Musayev F. N., di Salvo M. L., Ko T. P., Gandhi A. K., Goswami A., Schirch V. and Safo M. K. Crystal Structure of human pyridoxal kinase: structural basis of M(+) and M(2+) activation. *Protein Sci.,* **2007,** *16,* 2184-2194.

10. Mccormick D. B., and Snell E. E. Pyridoxal phosphokinases. II. Effects of inhibitors. *J. Biol. Chem,* **1961**, *236***,** 2085-2088.

11. Li M. H., Kwok F., Chang W. R., Liu S. Q., Lo S. C., Zhang J. P., Jiang T. and Liang D. C. Conformational changes in the reaction of pyridoxal kinase. *J. Biol. Chem***, 2004**, *279***,** 17459-17465.

12. Li M. H., Kwok F., Chang W. R., Lau C. K., Zhang J. P., Lo S. C., Jiang T. and Liang D. C. Crystal structure of brain pyridoxal kinase, a novel member of the ribokinase superfamily. *J. Biol. Chem,* **2002**, *277***,** 46385-46390.

13. Churchich J. E., and Wu C. Brain pyridoxal kinase. Mechanism of substrate addition, binding of ATP, and rotational mobility of the inhibitor pyridoxaloxime. *J. Biol. Chem.,* **1981**, *256***,** 780-784.

14. Yang Y., Tsui H. C., Man T. K. and Winkler M. E. Identification and function of the pdxY gene, which encodes a novel pyridoxal kinase involved in the salvage pathway of pyridoxal 5'-phosphate biosynthesis in Escherichia coli K-12. *J. Bacteriol.,* **1998,** *180*, 1814-1821.

15. Yang Y., Zhao G. and Winkler M. E. Identification of the pdxK gene that encodes pyridoxine (vitamin B6) kinase in Escherichia coli K-12. *FEMS Microbiol. Lett.* **1996** , *141***,** 89-95.

16. Gandhi, A.K.; Ghatge, M.; Musayev, F.N.; Sease, A.; Aboagye, S.O; Salvo, M.; Schirch, V. and Safo, M.K. Kinetic and Structural Studies of the Role of the Active Site Residue Asp235 of Pyridoxal Kinase. *Biochem Biophy Res Commun.*, **2009,** *381***,** 12-15.

17. Safo M. K., Mathews I., Musayev F. N., di Salvo M. L., Thiel D. J., Abraham D. J. and Schirch V. X-ray structure of Escherichia coli pyridoxine 5'-phosphate oxidase complexed with FMN at 1.8 A resolution. *Structure,* **2000***, 8***,** 751-762.

18. Musayev F. N., Di Salvo M. L., Ko T. P., Schirch V. and Safo M. K. Structure and properties of recombinant human pyridoxine 5'-phosphate oxidase. *Protein Sci.,* **2003,** *12***,** 1455-1463.

19. Yang E. S., and Schirch V. Tight binding of pyridoxal 5'-phosphate to recombinant Escherichia coli pyridoxine 5'-phosphate oxidase. *Arch. Biochem. Biophys.* **2000,** *377,* 109-114.

20. John R. A. Pyridoxal phosphate-dependent enzymes. *Biochim. Biophys. Acta,* **1995,** *1248,* 81-96.

21. McCormick, D. B. Biochemistry of coenzymes. In encyclopedia of molecular biology and molecular medicine (Meyers, R. A., ed.), 1996**,** pp. 396-406, VCH, Weinheim, Germany,

22. Leklem, J. E. Vitamin B-6 in handbook of vitamins (Machlin, L., ed.), 1991**,** pp. 341-378, Marcel Decker Inc., New York,

23. Jansonius J. N. Structure, evolution and action of vitamin B6-dependent enzymes. *Curr. Opin. Struct. Biol.* **1998,** *8,* 759-769.

24. Eliot A. C., Kirsch J. F. Pyridoxal phosphate enzymes: mechanistic, structural, and evolutionary considerations. *Annu. Rev. Biochem.* **2004**, 73**,** 383-415.

25. Percudani R., Peracchi A. A genomic overview of pyridoxal-phosphate-dependent enzymes. *EMBO Rep.* **2003**, *4***,** 850-854.

26. Mehta P. K., Christen P. The molecular evolution of pyridoxal-5'-phosphate-dependent enzymes. *Adv. Enzymol. Relat. Areas Mol. Biol.,* **2000,** *74***,** 129-184.

27. Christen P., Mehta P. K. From cofactor to enzymes. The molecular evolution of pyridoxal-5'-phosphate-dependent enzymes. *Chem. Rec. ,* **2001**, *1***,** 436-447.

28. Kim Y. T., Kwok F. and Churchich J. E. Interactions of pyridoxal kinase and aspartate aminotransferase emission anisotropy and compartmentation studies. *J. Biol. Chem.,* **1988,** *263,* 13712-13717. .

29. Cheung P. Y., Fong C. C., Ng K. T., Lam W. C., Leung Y. C., Tsang C. W., Yang M. and Wong M. S. Interaction between pyridoxal kinase and pyridoxal-5-phosphate-dependent enzymes. *J. Biochem.* **, 2003**, *134,* 731-738.

30. Bohme I., and Luddens H. The inhibitory neural circuitry as target of antiepileptic drugs. *Curr. Med. Chem.* **2001**, *8***,** 1257-1274.

31. Lloyd K. G., Munari C., Worms P., Bossi L., Bancaud J., Talairach J. and Morselli P. L. The role of GABA mediated neurotransmission in convulsive states. *Adv. Biochem. Psychopharmacol.,* **1981**, *26***,** 199-206.

32. Nishino N., Fujiwara H., Noguchi-Kuno S. A. and Tanaka C. GABAA receptor but not muscarinic receptor density was decreased in the brain of patients with Parkinson's disease. *Jpn. J. Pharmacol.,* **1988**, *48,* 331-339.

33. Aoyagi T., Wada T., Nagai M., Kojima F., Harada S., Takeuchi T., Takahashi H., Hirokawa K. and Tsumita T. Increased gamma-aminobutyrate aminotransferase activity in brain of patients with Alzheimer's disease. *Chem. Pharm. Bull. (Tokyo) ,* **1990**, *38,* 1748-1749.

34. Butterworth J., Yates C. M. and Simpson J. Phosphate-activated glutaminase in relation to Huntington's disease and agonal state. *J. Neurochem.,* **1983,** *41,* 440-447.

35. Schrag A. Psychiatric aspects of Parkinson's disease--an update. *J. Neurol.,* **2004,** *251***,** 795-804.

36. Snyder S. H., and Ferris C. D. Novel neurotransmitters and their neuropsychiatric relevance. *Am. J. Psychiatry,* **2000**, *157***,** 1738-1751.

37. Haas H., Panula P. The role of histamine and the tuberomamillary nucleus in the nervous system. *Nat. Rev. Neurosci. ,* **2003** , *4,* 121-130.

38. Ohtsu H., and Watanabe T. New functions of histamine found in histidine decarboxylase gene knockout mice. *Biochem. Biophys. Res. Commun.,* **2003,** *305***,** 443-447.

39. Perry C., Yu S., Chen J., Matharu K. S. and Stover P. J. Effect of vitamin B6 availability on serine hydroxymethyltransferase in MCF-7 cells. *Arch. Biochem. Biophys.,* **2007**, *462***,** 21-27.

40. Sharp P. S., Rainbow S. and Mukherjee S. Serum levels of low molecular weight advanced glycation end products in diabetic subjects. *Diabet. Med. ,* **2003,** *20***,** 575-579.

41. Salazar P., Tapia R. Seizures induced by intracerebral administration of pyridoxal-5'-phosphate: effect of GABAergic drugs and glutamate receptor antagonists. *Neuropharmacology,* **2001***, 41***,** 546-553.

42. Chung J. Y., Choi J. H., Hwang C. Y. and Youn H. Y. Pyridoxine induced neuropathy by subcutaneous administration in dogs. *J. Vet. Sci.,* 2008*, 9***,** 127-131.

43. Gdynia H. J., Muller T., Sperfeld A. D., Kuhnlein P., Otto M., Kassubek J. and Ludolph A. C. Severe sensorimotor neuropathy after intake of highest dosages of vitamin B6. *Neuromuscul. Disord. ,* **2008**, *18***,** 156-158.

44. Scott K., Zeris S. and Kothari M. J. Elevated B6 levels and peripheral neuropathies. *Electromyogr. Clin. Neurophysiol. ,* **2008,** *48***,** 219-223.

45. Perry T. A., Weerasuriya A., Mouton P. R., Holloway H. W. and Greig N. H. Pyridoxine-induced toxicity in rats: a stereological quantification of the sensory neuropathy. *Exp. Neurol. ,* **2004**, *190***,** 133-144.

46. Albin R. L., Albers J. W., Greenberg H. S., Townsend J. B., Lynn R. B., Burke J. M.,Jr and Alessi A. G. Acute sensory neuropathy-neuronopathy from pyridoxine overdose. *Neurology,* **1987***, 37***,** 1729-1732.

47. Bartzatt R., and Beckmann J. D. Inhibition of phenol sulfotransferase by pyridoxal phosphate. *Biochem. Pharmacol.* 1994, *47***,** 2087-2095.

48. Foca F. J. Motor and sensory neuropathy secondary to excessive pyridoxine ingestion. *Arch. Phys. Med. Rehabil.,* 1985, **66,** 634-636.

49. Morra M., Philipszoon H. D., D'Andrea G., Cananzi A. R., L'Erario R. and Milone F. F. Sensory and motor neuropathy caused by excessive ingestion of vitamin B6: a case report. *Funct. Neurol.,* **1993**, *8***,** 429-432.

50. Schaeffer M. C. Excess dietary vitamin B-6 alters startle behavior of rats. *J. Nutr. ,* **1993** , *123***,** 1444-1452.

51. Clayton P. T. B6-responsive disorders: a model of vitamin dependency. *J. Inherit. Metab. ,* **2006**, *29***,** 317-326.

52. Morris M. S., Picciano M. F., Jacques P. F. and Selhub J. Plasma pyridoxal 5'-phosphate in the US population: the National Health and Nutrition Examination Survey, 2003-2004. *Am. J. Clin. Nutr.* **2008** , *87,* 1446-1454.

53. Steichen O., Martinez-Almoyna L. and De Broucker T. Isoniazid induced neuropathy: consider prevention. *Rev. Mal. Respir.,* **2006**, *23***,** 157-160.

54. Kuwahara H., Noguchi Y., Inaba A. and Mizusawa H. Case of an 81-year-old woman with theophylline-associated seizures followed by partial seizures due to vitamin B6 deficiency. *Rinsho Shinkeigaku,* **2008** , *48***,** 125-129.

55. Laine-Cessac P., Cailleux A. and Allain P. Mechanisms of the inhibition of human erythrocyte pyridoxal kinase by drugs. *Biochem. Pharmacol.* **1997**, *54***,** 863-870.

56. Ubbink J. B., Delport R., Bissbort S., Vermaak W. J. and Becker P. J. Relationship between vitamin B-6 status and elevated pyridoxal kinase levels induced by theophylline therapy in humans. *J. Nutr. ,* **1990**, *120***,** 1352-1359.

57. Delport R., Ubbink J. B., Vermaak W. J. and Becker P. J. Theophylline increases pyridoxal kinase activity independently from vitamin B6 nutritional status. *Res. Commun. Chem. Pathol. Pharmacol. ,* **1993**, *79***,** 325-333.

58. Seto T., Inada H., Kobayashi N., Tada H., Furukawa K., Hayashi K., Hattori H., Matsuoka O. and Isshiki G. Depression of serum pyridoxal levels in theophylline-related seizures. *No to. Hattatsu.,* **2000***, 32***,** 295-300.

59. Weir M. R., Keniston R. C., Enriquez JI S. and McNamee G. A. Depression of vitamin B6 levels due to dopamine. *Vet. Hum. Toxicol. ,* **1991**, *33,* 118-121.

60. Alao A. O., Yolles J. C. Isoniazid-induced psychosis. *Ann. Pharmacother.,* **1998** , *32***,** 889-891.

61. Bonner A. B., Peterson S. L. and Weir M. R. Seizures induced by theophylline and isoniazid in mice. *Vet. Hum. Toxicol.* **1999**, *41***,** 175-177.

62. Tutor-Crespo M. J., Hermida J. and Tutor J. C. Activation of serum aminotransferases by pyridoxal-5' -phosphate in epileptic patients treated with anticonvulsant drugs. *Clin. Biochem.,* **2004**, *37***,** 714-717.

63. Delport R., Ubbink J. B., Serfontein W. J., Becker P. J. and Walters L. Vitamin B6 nutritional status in asthma: the effect of theophylline therapy on plasma pyridoxal-5'-phosphate and pyridoxal levels. *Int. J. Vitam. Nutr. Res.,* **1988**, *58***,** 67-72.

64. Fiehe K., Arenz A., Drewke C., Hemscheidt T., Williamson R. T. and Leistner E. Biosynthesis of 4'-O-methylpyridoxine (Ginkgotoxin) from primary precursors. *J. Nat. Prod.,* **2000**, *63***,** 185-189.

65. Hahn I. H., Varney S. Pyridoxine treatment for seizures induced by theophylline and isoniazid? *Vet. Hum. Toxicol.,* **1999**, *41***,** 342.

66. Glenn G. M., Krober M. S., Kelly P., McCarty J. and Weir M. Pyridoxine as therapy in theophylline-induced seizures. *Vet. Hum. Toxicol.,* 1995, 37**,** 342-345.

67. Rasul C. H., and Das S. C. Vitamin B6 supplementation with isoniazid therapy. *Trop. Doct.* **2000**, *30***,** 55-56.

68. Sandyk R., Pardeshi R. Pyridoxine improves drug-induced parkinsonism and psychosis in a schizophrenic patient. *Int. J. Neurosci.,* **1990**, *52***,** 225-232.

69. Santucci K. A., Shah B. R. and Linakis J. G. Acute isoniazid exposures and antidote availability. *Pediatr. Emerg. Care,* **1999**, *15*, 99-101.

70. Bach S., Knockaert M., Reinhardt J., Lozach O., Schmitt S., Baratte B., Koken M., Coburn S. P., Tang L., Jiang T., Liang D. C., Galons H., Dierick J. F., Pinna L. A., Meggio F., Totzke F., Schachtele C., Lerman A. S., Carnero A., Wan Y., Gray N. and Meijer L. Roscovitine targets, protein kinases and pyridoxal kinase. *J. Biol. Chem. ,* **2005**, *280,* 31208-31219.

71. Tang L., Li M. H., Cao P., Wang F., Chang W. R., Bach S., Reinhardt J., Ferandin Y., Galons H., Wan Y., Gray N., Meijer L., Jiang T. and Liang D. C. Crystal structure of pyridoxal kinase in complex with roscovitine and derivatives. *J. Biol. Chem.,* **2005**, *280***,** 31220-31229.

72. Aaltonen J., Bjorses P., Sandkuijl L., Perheentupa J. and Peltonen L. An autosomal locus causing autoimmune disease: autoimmune polyglandular disease type I assigned to chromosome 21. *Nat. Genet.,* **1994**, *8***,** 83-87.

73. Mills P. B., Surtees R. A., Champion M. P., Beesley C. E., Dalton N., Scambler P. J., Heales S. J., Briddon A., Scheimberg I., Hoffmann G. F., Zschocke J. and Clayton P. T. Neonatal epileptic encephalopathy caused by mutations in the PNPO gene encoding pyridox(am)ine 5'-phosphate oxidase. *Hum. Mol. Genet.,* **2005**, *14,* 1077-1086.

74. Ruiz A., Garcia-Villoria J., Ormazabal A., Zschocke J., Fiol M., Navarro-Sastre A., Artuch R., Vilaseca M. A. and Ribes A. A new fatal case of pyridox(am)ine 5'-phosphate oxidase (PNPO) deficiency. *Mol. Genet. Metab.,* **2008**, *93***,** 216-218.

75. Hoffmann G. F., Schmitt B., Windfuhr M., Wagner N., Strehl H., Bagci S., Franz A. R., Mills P. B., Clayton P. T., Baumgartner M. R., Steinmann B., Bast T., Wolf N. I. and Zschocke J. Pyridoxal 5'-phosphate may be curative in early-onset epileptic encephalopathy. *J. Inherit. Metab. Dis.,* **2007**, *30***,** 96-99.

76. Clayton P. T., Surtees R. A., DeVile C., Hyland K. and Heales S. J. Neonatal epileptic encephalopathy. *Lancet* **, 2003***, 361***,** 1614.

77. Musayev F. N., di Salvo M. L., Saavedra M.A, Contestabile R., Ghatge, M.S., Schirch V. and Safo M. K. Molecular basis of reduced pyridoxine 5'-phosphate oxidase catalytic activity in neonatal epileptic encephalopathy disorder. *J Biol Chem.* , **2009**, *284*, 30949-56.

78. Adams J. B., George F. and Audhya T. Abnormally high plasma levels of vitamin B6 in children with autism not taking supplements compared to controls not taking supplements. *J. Altern. Complement. Med.,* **2006,** *12***,** 59-63.

79. Mousain-Bosc M., Roche M., Polge A., Pradal-Prat D., Rapin J. and Bali J.P. Improvement of neurobehavioral disorders in children supplemented with magnesium-vitamin B6. II. Pervasive developmental disorder-autism., **2006,** *19,* 53.

80. Rajesh R., and Girija A. S. Pyridoxine-dependent seizures: a review. *Indian Pediatr.,* **2003,** *40***,** 633-638.

81. Nogovitsina O. R., Levitina E. V. Effect of MAGNE-B6 on the clinical and biochemical manifestations of the syndrome of attention deficit and hyperactivity in children. *Eksp. Klin. Farmakol.,* **2006***, 69***,** 74-77.

82. Herrmann W., Lorenzl S. and Obeid R. Review of the role of hyperhomocysteinemia and B-vitamin deficiency in neurological and psychiatric disorders--current evidence and preliminary recommendations. *Fortschr Neurol. Psychiatr,* **2007,** *75***,** 515-527.

83. Fuso A., Nicolia V., Cavallaro R. A., Ricceri L., D'Anselmi F., Coluccia P., Calamandrei G. and Scarpa S. B-vitamin deprivation induces hyperhomocysteinemia and brain S-adenosylhomocysteine, depletes brain S-adenosylmethionine, and enhances PS1 and BACE expression and amyloid-beta deposition in mice. *Mol. Cell. Neurosci. ,* **2008**, *37,* 731-746.

84. Leyland D. M., Beynon R. J. The expression of glycogen phosphorylase in normal and dystrophic muscle. *Biochem. J. ,* **1991**, *278,* 113-117.

85. Spinneker A., Sola R., Lemmen V., Castillo M. J., Pietrzik K. and Gonzalez-Gross M. Vitamin B6 status, deficiency and its consequences--an overview. *Nutr. Hosp.***, 2007,** *22***,** 7-24.

86. Gupta A., Moustapha A., Jacobsen D. W., Goormastic M., Tuzcu E. M., Hobbs R., Young J., James K., McCarthy P., van Lente F., Green R. and Robinson K. High homocysteine, low folate, and low vitamin B6 concentrations: prevalent risk factors for vascular disease in heart transplant recipients. *Transplantation***, 1998***, 65***,** 544-550.

87. Jacobsen D. W. Homocysteine and vitamins in cardiovascular disease. *Clin. Chem.,* **1998,** *44,* 1833-1843.

88. Meydani S. N., Ribaya-Mercado J. D., Russell R. M., Sahyoun N., Morrow F. D. and Gershoff S. N. Vitamin B-6 deficiency impairs interleukin 2 production and lymphocyte proliferation in elderly adults. *Am. J. Clin. Nutr.,* **1991**, *53,* 1275-1280.

89. Adams J. B., and Holloway C. Pilot study of a moderate dose multivitamin/mineral supplement for children with autistic spectrum disorder. *J. Altern. Complement. Med.,* **2004**, *10***,** 1033-1039.

90. Coburn S. P., Mahuren J. D. and Schaltenbrand W. E. Increased activity of pyridoxal kinase in tongue in Down's syndrome. *J. Ment. Defic. Res. ,* **1991**, *35***,** 543-547.

91. Song H., Ueno S., Numata S., Iga J., Shibuya-Tayoshi S., Nakataki M., Tayoshi S., Yamauchi K., Sumitani S., Tomotake T., Tada T., Tanahashi T., Itakura M. and Ohmori T. Association between PNPO and schizophrenia in the Japanese population. *Schizophr. Res.,* **2007,** *97,* 264-270.

92. Di Salvo M. L., Hunt S. and Schirch V. Expression, purification, and kinetic constants for human and Escherichia coli pyridoxal kinases. *Protein Expr. Purif.* **, 2004**, *36***,** 300-306.

93. Claude, J.B., Suhre, K., Notredame, C., Claverie, J.-M., and Abergel, C. CaspR: A Web server for automated molecular replacement using homology modeling. *Nucleic Acids Res*., **2004**, *32***,** W606–W609.

94. Notredame, C., Higgins, D., and Heringa, J. T-Coffee: A novel method for fast and accurate multiple sequence alignment. *J. Mol. Biol.* , **2000**, *302***,** 205– 217.

95. Sali, A. and Blundell, T.L. Comparative protein modelling by satisfaction of spatial restraints. *J. Mol. Biol.* , **1993**, *234,* 779–815.

96. Navaza, J. AMoRe: An automated package for molecular replacement. *Acta Crystallogr.*, **1994***, A50***,** 157–163.

97. Brunger, A.T., Adams, P.D., Clore, G.M., DeLano, W.L., Gros, P., Grosse-Kunstleve, R.W., Jiang, J.-S., Kuszewski, J., Nilges, M., Pannu, N.S., et al. Crystallography & NMR system: A new software suite for macromolecular structure determination. *Acta Crystallogr.* , **1998**, *D54***,** 905–921.

98. Siegel, I.H. Enzyme Kinetics: Behavior and Analysis of Rapid Equilibrium and Steady-State Enzyme Systems. **1975,** *274-283.*

99. Toney, M.D., Hohenester, E., Cowan, S.W., and Jansonius, J.N. Dialkylglycine decarboxylase structure: Bifunctional active site and alkali metal sites. *Science*, **1993,** *261,* 756–759.

100. Toney, M.D., Hohenester, E., Keller, J.W., and Jansonius, J.N. Structural and mechanistic analysis of two refined crystal structures of the pyridoxal phosphate-dependent enzyme dialkylglycine decarboxylase. *J. Mol. Biol.,* **1995,** *245,* 151–179.

101. Pineda, A. O., Carrell, C. J., Bush, L. A., Prasad, S., Caccia, S., Chen, Z. -W., Mathews, F. S., and Di Cera, E. Molecular dissection of Na^+ binding to thrombin. *J. Biol. Chem.,* **2004***, 279***,** 31842–31853.

102. Larsen, T. M., Benning, M. M., Rayment, I., and Reed, G. H. Structure of the bis(Mg^{2+})-ATP-oxalate complex of the rabbit muscle pyruvate kinase at 2.1 A resolution: ATP binding over a barrel. *Biochemistr*y, **1998**, *37***,** 6247–6255.

103. Page, M. J., and Di Cera, E. Role of Na+ and K+ in enzyme function. *Physiol. Rev.,* **2006**, *86***,** 1049-1092.

104. Collins, K. D. Sticky ions in biological systems. *Proc. Natl. Acad. Sci. USA,* **1995,** *92***,** 5553–5557.

105. Collins, K. D. Charge density-dependent strength of hydration and biological structure. *Biophy*s. *J.* **1997**, *72***,** 65–76.

106. Collins, K. D. Ion hydration: implications for cellular function, polyelectrolytes, and protein crystallization. *Biophys. Chem.,* **2006,** *119***:** 271– 281.

107. Zhang, Y., M. Dougherty, D. M. Downs, and S. E. Ealick. Crystal structure of an aminoimidazole riboside kinase from Salmonella enterica: implications for the evolution of the ribokinase superfamily. *Structure,* **2004**, *12***,**1809-1821.

108. Di Cera, E. A structural perspective on enzymes activated by monovalent cations, *J. Biol. Chem.,* **2006**, *281***,**1305-1308.

109. Yamada, T., Komoto, J., Takata, Y., Ogawa, H., Pitot, H. C., and Takusagawa, F. Crystal structure of serine dehydratase from rat liver. *Biochemistry,* **2003**, *42***,** 12854-12865.

110. Isupov, M. N., Antson, A. A., Dodson, E. J., Dodson, G. G., Dementieva, I. S., Zakomirdina, L. N., Wilson, K. S., Dauter, Z., Lebedev, A. A., and Harutyunyan, E. H. Crystal structure of tryptophanase. *J. Mol. Biol.* , **1998**, *276***,** 603-623.

111. Cambillau, C. and Horjales, E.TOM: a frodo subpackage for protein-ligand fitting with interactive energy minimization*, J. Mol. Graph.,* **1987,** *5,* 74–177.

112. Emsley, P. and Cowtan, K. COOT: model-building tools for molecular graphics, *Acta Cryst.* , **2004,** *D 60*, 2126–2132.

113. Selli, A.; Crociani, F.; Matteuzzi, D. and Crisetig, G. Feedback inhibition of homoserine dehydrogenase and threonine deaminase in the genus *Bifidobacterium. Current Microbiology,* **1986***, 13,* 33-38.

114. Rognes, S. E.; Bright, S.W.J. and Miflin, B. J. Feedback-insensitive aspartate kinase isoenzymes in barley mutants resistant to lysine plus threonine. *Planta,* **1983,** *157,* 32-38.

VITA

Amit K. Gandhi was born on 19th July, 1980 in Raipur, Chattisgard, India. He received his Bachelor and Master of Pharmacy degree from Rajiv Gandhi University, Indore, India in 2001 and 2003, respectively. He joined Dr. Matrin K. Safo's research group in the Department of Medicinal Chemistry, School of Pharmacy at Virginia Commonwealth University in fall 2005. Amit received J. Doyle Smith Award, 2009 for achieving the greatest distinction in the areas of research, teaching, scholarship and service in the Department of Medicinal Chemistry at Virginia Commonwealth University.